The dissolution rates of naturally altered basalts at pH 3 and 120 °C: Implications for the in-situ mineralization of CO2 injected into the subsurface

Sylvain Delerce, Pascale Bénézeth, Jacques Schott, Eric Oelkers

The dissolution rates of naturally altered basalts at pH 3 and 120 °C: Implications for the in-situ mineralization of CO2 injected into the subsurface

Sylvain Delerce, Pascale Bénézeth, Jacques Schott, Eric H Oelkers

The dissolution rates of naturally altered basalts at pH 3 and 120 °C: Implications for the in-situ mineralization of CO_2 injected into the subsurface

Sylvain Delerce[1], Pascale Bénézeth[1], Jacques Schott[1], Eric H. Oelkers[2]

[1]Géosciences Environnement Toulouse, GET – CNRS – CNES – IRD – OMP – Université de Toulouse, Toulouse, France, 14 Avenue Edouard Belin, 31400 Toulouse, France

[2] Institute of Earth Sciences, University of Iceland, Sæmundargata 2, 102 Reykjavík, Iceland

Highlights

- Basalts of varying degrees of alteration were dissolved at pH 3 and 120 °C in mixed flow reactors
- Element release rates were one to three orders of magnitude slower than basaltic glass
- Rates were similar for all of the basalts despite different alteration conditions and mineralogies
- Rates still sufficiently fast to carbonate CO_2 in the subsurface, particularly at 120 °C or higher

Abstract

Due to their widespread distribution in the Earth's crust, it seems likely that altered basalts could be targeted for CO_2 storage via subsurface mineral carbonation. To assess the potential efficiency of this approach, the steady state release rates of major elements from a suite of altered basalts have been measured at pH 3, 120 °C, and far from equilibrium conditions. The dissolved rock samples have chemical compositions close to that of fresh basalt, but their mineralogy varies due to their alteration either at the Earth's surface or hydrothermal conditions at temperatures up to 250 °C. The studied altered basalts contain variable amounts of primary plagioclase and pyroxene, and substantial secondary clays, quartz, zeolites, epidote and chlorites as alteration phases. Despite their differing mineralogy, the steady-state element release rates of all of the altered basalts are similar to each other when normalized to geometric surface area, but one to three orders of magnitude slower than corresponding release rates of basaltic glass and fresh crystalline basalt, depending on the element and on whether the rates are normalized to initial BET or geometric surface area. If present in small amounts in the altered basalts, the calcite dissolved rapidly in the acidic reactive fluids, and did not contribute to the measured steady-state calcium release rates. Taken together, the results of this study indicate that altered basalt formations can provide sufficient divalent

cations for subsurface carbon mineralization. As the element release rates of these altered basalts are lower than those of basaltic glass or fresh crystalline basalt, efforts to carbonate subsurface altered basalts may be best targeted at systems having temperatures in excess of 100 °C to compensate for the lower reactivity of these rocks.

1. Introduction

The Earth's carbon cycle has been regulated over geological times by the feedback between atmospheric CO_2 concentration, surface temperature and silicate rock weathering (Walker et al., 1981; Berner et al., 1983; Brady and Carroll, 1994; Gislason et al., 2009). Silicate mineral weathering releases divalent cations able to react with atmospheric CO_2 to form stable carbonate minerals, thus sequestering carbon through a process called carbon mineralization. On average it is estimated that the natural weathering of silicates globally results in approximately 0.4GtCO_2/yr drawdown (Gaillardet et al., 1999). This process leads to long-term storage of the mineralized CO_2; the average residence time of carbonates in Earth's crust has been estimated to be more than 200 Myr (Berner, 2004).

Carbon mineralization may prove highly useful to remove CO_2 from the atmosphere as part of engineered carbon capture and storage strategies (Oelkers and Schott, 2005; Snæbjörnsdóttir et al., 2020; Okoko and Olaka, 2021). Efforts are currently under development to optimize carbon mineralization processes (Kelemen et al., 2020), both at Earth surface conditions via enhanced weathering (Köhler et al., 2010; Harrison et al., 2013; Kantola et al., 2017; Meysman and Montserrat, 2017; Fuhr et al., 2022), and in the subsurface (Kelemen et al., 2011, 2018; McGrail et al., 2017; Gislason et al., 2018; Snæbjörnsdóttir et al., 2020; Galeczka et al., 2022). Reactive rocks such as basalts and peridotites (Kelemen and Matter, 2008; Lacinska et al., 2017; Kelemen et al., 2018; Rigopoulos et al., 2018), and fine-grained materials such as mine tailings (Oskierski et al., 2013; Wilson et al., 2014; Turvey et al., 2018; Power et al., 2020; Lu et al., 2022; Stubbs et al., 2022) and steel slags (Huijgen et al., 2005; Pan et al., 2017; Mayes et al., 2018; Chukwuma et al., 2021) are of particular interest for carbon mineralization as they are relatively rich in carbonates forming cations and reactive to mildly acidic CO_2 charged water.

The CarbFix project demonstrated in a field scale pilot injection that it is possible to mineralize CO_2 upon its injection into fresh subsurface basalts in less than 2 years (Matter et al., 2016;

Gislason et al., 2018). This process was upscaled to capture and store the bulk of the carbon emissions at the Hellisheiði power plant by its injection into altered basalts at temperatures of ~250^{o}C (Gunnarsson et al., 2018; Clark et al., 2020). Plans are currently underway to adopt this approach at other sites (Galeczka et al., 2022), and the subsurface mineralization of basalts have been proposed in other regions including the Deccan traps of India (Shrivastava et al., 2016; Liu et al., 2022) and the East African Rift basalts (Okoko and Olaka, 2021). Since mafic rocks, such as basalt, are widely distributed in the Earth's crust and ocean floor, the potential storage capacity of subsurface mineralization is vast. Estimates of submarine basalt carbon storage potential range from 1,000 to 250,000 $GtCO_2$ (National Academies of Sciences Engineering and Medicine, 2019; Snæbjörnsdóttir et al., 2020). Globally, the availability of fresh basaltic rocks is limited to active volcanic systems and rift zones. Far more widespread are basaltic rocks that have been altered through heat and/or the passage of hydrothermal fluids. Such rocks could provide new targets for carbon storage through subsurface mineralization (Liu et al., 2019). This study was motivated to assess the relative reactivity of altered basalts to determine the efficiency of carbonating these rocks as a function of their degree of alteration.

Numerous past studies have reported the dissolution rates of secondary basaltic minerals including chlorites (Ross, 1967; Malmström et al., 1996; Gustafsson and Puigdomenech, 2003; Lowson et al., 2005), zeolites (Ragnarsdóttir, 1993; Savage et al., 1993; Hartman and Fogler, 2005), epidote (Kalinowski et al., 1998; Marieni et al., 2021), and quartz (Brady and Walther, 1990; House and Orr, 1992; Berger et al., 1994; Brantley, 2008). Other experimental studies have considered the dissolution of whole rocks (Schaef and McGrail, 2009; Schaef et al., 2010; Critelli et al., 2014; Marieni et al., 2020) and/or explored the potential of rock dissolution for subsurface CO_2 geologic storage (Adeoye et al., 2017; Kumar et al., 2017; Marieni and Oelkers, 2018; Menefee et al., 2018). These studies suggest that (i) the dissolution rates of minerals in whole rocks tend to be similar to those of the individual minerals and (ii) calcium bearing secondary phases can be favorable for carbon mineralization by releasing significant amounts of calcium to the fluid phase. Building upon these past works, the element release rates from 9 different basaltic rocks including surface weathered and hydrothermally altered basalts have been measured in the present study at far from equilibrium in mixed flow reactors at 120 °C and pH 3. Two additional non-basaltic rocks originating from a geothermal field were also

dissolved at these conditions for comparison. The obtained element release rates have then been used to explore the feasibility of subsurface CO_2 mineral storage in altered basaltic rocks.

2. Material and methods

The rock samples considered in this study were selected to explore the effects of contrasting alteration profiles on basalt reactivity and their mineral carbonation potential. These samples consisted of eight altered basalts from Iceland, one sample from the Deccan traps in India, and two non-basaltic rock samples from a geothermal field in Western Turkey. The sampling location of these rocks are provided in Figure 1.

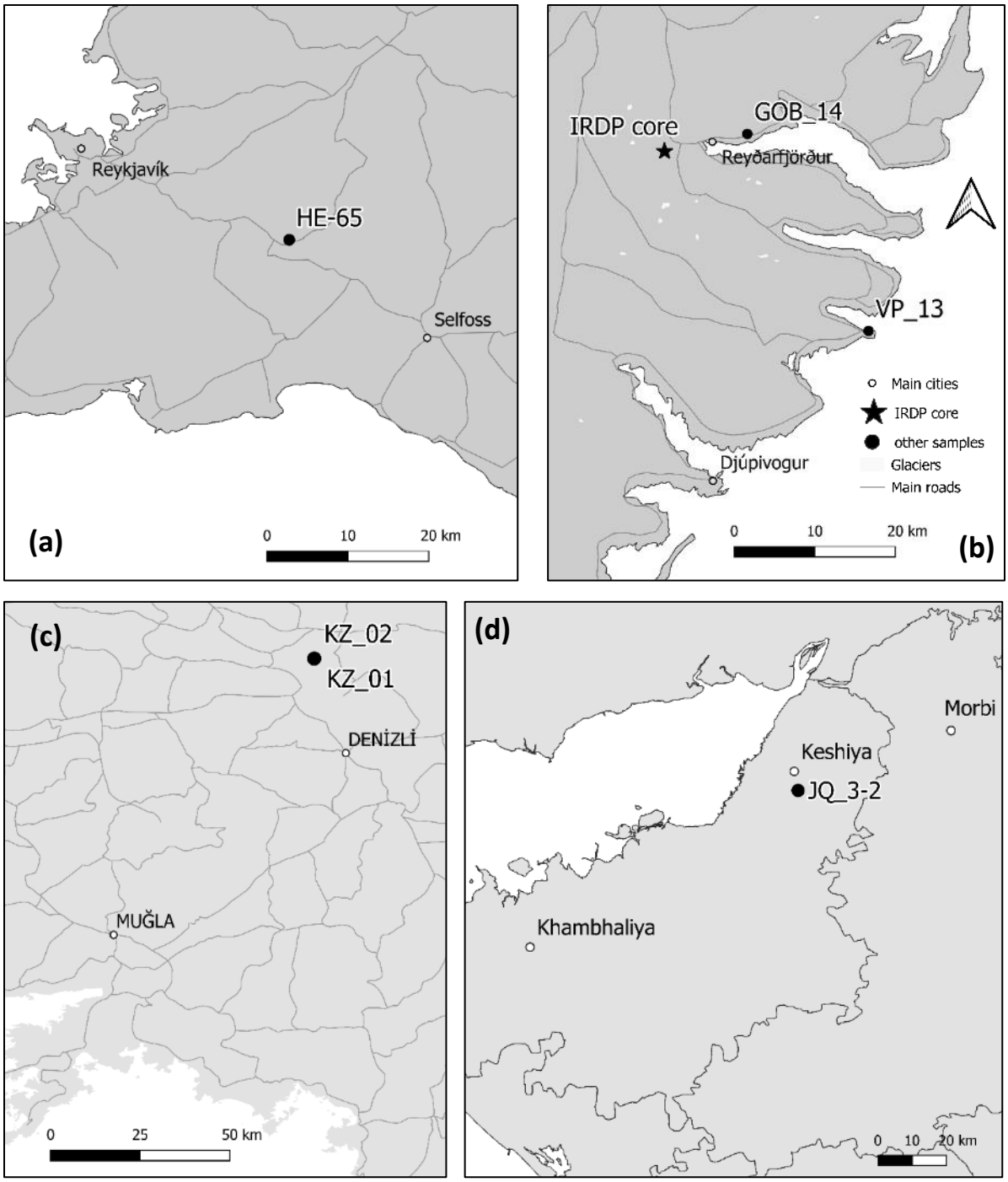

Figure 1 : Location maps showing the origin of the different samples used in this study: (a) western Iceland, (b) eastern Iceland, (c) western Turkey and (d) Eastern India.

Five of the Icelandic samples were taken from a two kilometer long drill core recovered during the Iceland Research Drilling Project (IRDP) near Reyðarfjörður, eastern Iceland, during the summer of 1978 (Fridleifsson et al., 1982; Robinson et al., 1982a). The core cut through a succession of lava flows with their corresponding flow tops, breccias and massive layers (Mehegan et al., 1982; Robinson et al., 1982b). The five studied samples from this core were selected from brecciated flow tops and were originally at depths ranging from 480 to 1800 m.

The names of the samples from this core refer to the number of the box and the sub-section from which the sample was obtained. Flow tops are commonly more porous than the dense interiors of lava flows and thus more highly altered (McGrail et al., 2006). Such samples are, therefore, more likely to be representative of the rocks encountered along the flow path of the CO_2 injected into basaltic rocks. Three samples from the uppermost part of the Reyðarfjörður core experienced zeolite facies alteration. Two of these samples, B83S3 and B87S4, contain minor calcite. The deepest samples, B261S4 and B316S3, experienced epidote facies alteration. One Icelandic sample was provided by CarbFix and comes from a depth of 1506 m in the HE-65 well in Hellisheiði. This sample is a dense, fine-grained crystalline basalt having experienced actinolite facies alteration. Two samples were collected from the surface of eastern Iceland. One of these samples, GOB_14, was collected from an approximately 9 Myr old microcrystalline basalt outcrop belonging to the Grjótá olivine basalt group (GOB) previously described by Óskarsson and Riishuus (2013). This sample is representative of the evolved end of the group where olivine is marginal. The other surface sample, VP_13, is an approximately 13 Myr old porphyritic microcrystalline basalt. It was sampled from an outcrop belonging to the Vindháls porphyritic group (VP), which has been previously described by Walker (1958). The last basaltic sample originates from the Deccan traps formation (India), more specifically from a surface outcrop near the town of Keshiya representative of the lithology of a potential basalt-hosted subsurface carbon storage reservoir. In addition, two non-mafic samples provided by the Pamukkale University were collected from outcrops representative of the lithology of the Kizildere (KZ) geothermal field in Western Turkey. The first is a marble and the second is a mica schist. These latter samples serve as a comparison to the behavior of the mafic rocks considered in this experimental study. A summary of the samples involved in this study is given in Table 1.

Table 1 : Summary of the samples used in this study

Origin	*Sample Name*	*Type of sample*	*Depth of sample (m)*	*Latitude*	*Longitude*
IRDP core	B83S3	Core	487	65.026117	-14.346117
	B87S4		512		
	B130S2		758		
	B216S4		780		
	B316S3		1125		
Hellisheidi	HE-65		1506	64.041317	-21.3612
Eastern Iceland	GOB_14	Outcrop	-	65.02955	-14.125199
	VP_13		-	-64.809476	-13.849058
Deccan traps	JQ_3-2		-	22.648438	70.406199
Kizildere geothermal field	KZ_01		-	38.076109	28.988003
	KZ_02		-	38.075671	28.987239

Latitude and longitude are given in decimal degrees.

2.1. Sample preparation and characterization

A diamond saw was used to cut all the investigated rock samples and to remove their surfaces to eliminate foreign materials or altered rims. The samples were then dried several days before being crushed by hammer and then ground using an agate vibrating-disc mill. The resulting powders were dry sieved to recover the 40-150 µm fraction except for sample HE-65, where the 40-125µm fraction was collected and for samples KZ_01 and KZ_02, where the 40-200 µm fraction was collected. The prepared size fractions were then cleaned to remove fine particles using ultrapure deionized water (DIW) and gravitational setting, and subsequently further cleaned using an ultrasonic bath with the powder in DIW and then ethanol. Depending on the sample and how many fines it contained, 5 to 20 cleaning cycles using DIW and gravitational setting and 5 to 10 cleaning cycles using the ultrasonic bath with DIW and ethanol were required to remove the fine particles. The grains were considered to be clean when the fluid phase after the ultrasonic cleaning cycle was clear to the eye. The cleaned powders were finally oven dried at 50 °C for several days. Representative scanning electron microscope (SEM) images of the prepared powders are shown in Figure 2. The

cleaned rock powders are free from fine particles and have sizes corresponding to the selected size fraction. Most of the B130S2 grains in the images exhibit significant surface roughness.

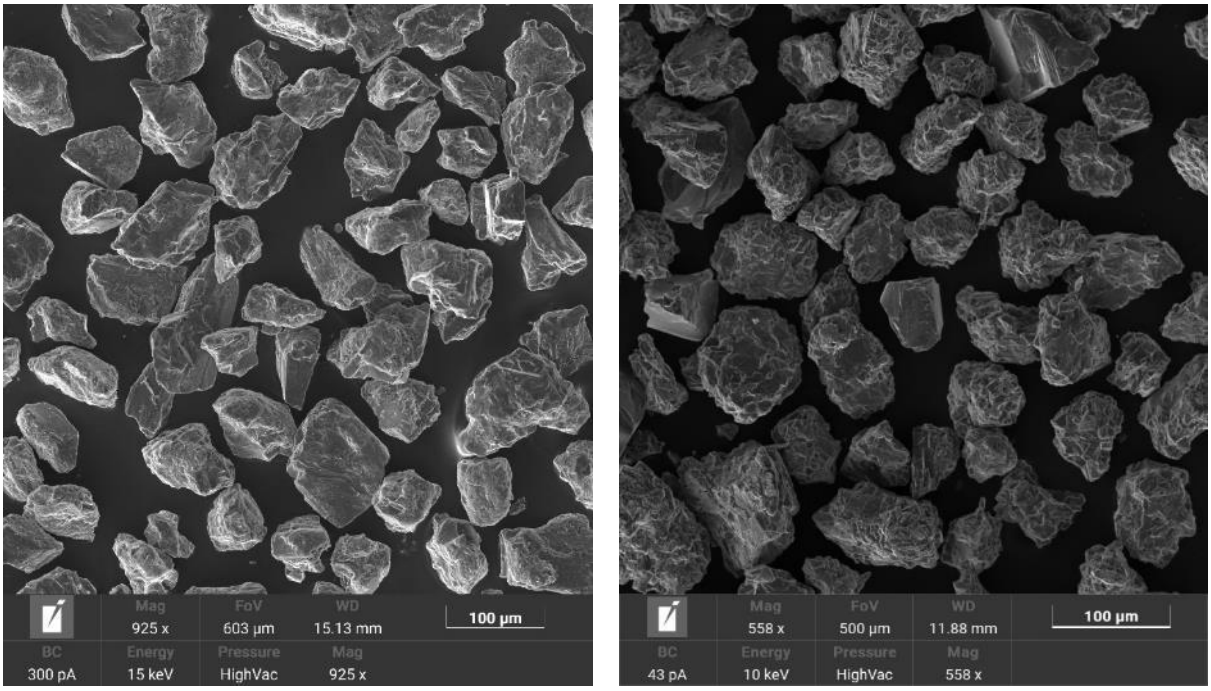

Figure 2 : SEM images of prepared samples HE-65 (left) and VP_13 (right). The grains are free of fine particles and have a grain size corresponding to the 40-150 µm size fraction.

The specific surface area of the rock powders was measured using the Brunauer-Emmet-Teller (BET) method with 11 adsorption points using the Quantachrome Autosorb-1MP gas sorption system at Géosciences Environment Toulouse. Either krypton or nitrogen adsorption was used depending on the measured surface area, which are reported in Table 2. The uncertainties of these measurements are estimated to be ±15% based on repeated analyses. The geometric surface area was also calculated for each sample using (Tester et al., 1994) :

$$A_{geo} = \frac{6}{\rho * d_{eff}} \quad (1)$$

where ρ refers to the rock density of the rock and d_{eff} to the effective particle diameter. The density of all samples was assumed to be 2.9 and d_{eff} was calculated *using:*

$$d_{eff} = \frac{d_{max} - d_{min}}{\ln(\frac{d_{max}}{d_{min}})} \quad (2)$$

where d_{max} and d_{min} correspond to the largest and smallest sieve mesh sizes used for particle separation, respectively.

Table 2 : Specific surface areas of the prepared rock powders used in the present study

Sample	*Size fraction (µm)*	*BET surface area ($m^2.g^{-1}$)*	*Geometric surface area ($m^2.g^{-1}$)*	*BET/GEO ratio**
B83S3	40-150	2.53	0.0249	102
B87S4	40-150	4.15	0.0249	167
B130S2	40-150	1.73	0.0249	70
B261S4	40-150	1.49	0.0249	60
B316S3	40-150	0.43	0.0249	17
HE-65	40-125	2.03	0.0277	73
GOB_14	40-150	1.60	0.0249	64
VP_13	40-150	4.98	0.0249	200
JQ_3-2	40-150	7.49	0.0249	301
KZ_01	40-200	0.29	0.0208	14
KZ_02	40-200	1.8	0.0208	86

* ratio of the measured BET surface area divided by the calculated geometric surface area for a rock sample.

Significant variations exist among the BET surface areas of the prepared rock powders. These variations could be attributed to the mineralogy of the samples. Several studies reported that chlorite and zeolite minerals exhibit high BET surface areas due to the presence of internal porosity (Yates, 1968; Valdés et al., 2006). Clays minerals are also noted to have large surface areas due to their characteristic shape (Murray and Quirk, 1990). Note the content of clay minerals were not measured directly in the sample considered in this study. The presence of clay minerals was identified in some of the samples as noted in Table 4, but not quantified. There is an ongoing debate in the literature on whether it is more instructive to use BET or geometric surface area to normalize dissolution rates (Brantley and Mellott, 2000; Gautier et al., 2001; Wolff-Boenisch et al., 2006; Marini, 2007; Schaef and McGrail, 2009; Heřmanská et al., 2022). Here, we dissolve natural rocks, which by nature are more complex systems than single pure minerals. Therefore, we report rates normalized to each of these surface areas.

The bulk chemical composition of the studied rock samples was measured by X-ray fluorescence spectrometry (XRF) using a S2 ranger Bruker spectrometer located at Géosciences Environnement Toulouse. The measured compositions are reported in Table 3.

Table 3 : Chemical composition of the samples as determined by XRF (wt%). The composition of Stapafell basaltic glass is added for comparison

Sample	B83S3	B87S4	B130S2	B261S4	B316S3	HE65_#2-2	GOB_14	VP_13	JQ_3-2	KZ_01	KZ_02	Basaltic glass*
SiO_2	49.27	49.87	55.71	45.48	56.53	46.1	45.27	42.82	49.05	14.29	69.7	48.12
TiO_2	2.66	2.13	1.86	2.19	1.89	3.14	2.21	2.71	0.73	0.09	0.52	1.56
Al_2O_3	11.37	10.46	10.26	9.32	9.76	12.59	13.21	14.01	12.77	1.55	14.32	14.62
Fe_2O_3	12.82	14.94	9.9	11.22	10.41	16.6	12.3	12.27	11.77	0.91	7.6	1.11
FeO	-	-	-	-	-	-	-	-	-	-	-	9.82
Mn_2O_3	0.17	0.18	0.23	0.25	0.15	0.29	0.21	0.2	0.29	-	-	-
MnO	-	-	-	-	-	-	-	-	-	0.04	0.07	0.19
CaO	7.49	6.61	4.72	8.77	12.32	10.12	10.53	9.2	10.16	44.08	0.76	11.84
MgO	3.81	6.81	2.03	5.83	4.02	5.28	6.72	4.29	5.42	1.58	0.79	9.08
Na_2O	3.42	0.75	2.33	0.08	0.21	2.47	2.41	2.6	1.46	0.07	0.46	1.97
K_2O	0.31	0.07	1.07	0.05	0.05	0.11	0.19	0.59	0.2	0.33	1.42	0.29
P_2O_5	0.32	0.33	0.54	0.32	0.32	0.46	0.35	0.42	0.24	-	0.18	0.2
SO_3	0.42	0.27	0.6	0.14	0	0.29	0.07	0.23	0	-	-	-
LOI	9.06	8.46	11.71	17.12	5.41	2.39	6.33	10.08	6.83	37.02	4.32	-
Total	101.12	100.88	100.96	100.77	101.07	99.84	99.8	99.42	98.92	99.96	100.14	98.8

*from (Oelkers and Gislason, 2001)

The chemical compositions of the rocks are characteristic of basalt. Note that the hydrothermally altered basalts show a higher silicon content and lower aluminum, magnesium and calcium contents than basaltic glass, except for sample B316S3 which has a higher calcium content. No consistent trends are evident for the iron content of the rocks. In line with their mineralogy, KZ_01 and KZ_02, a marble and a mica schist, have chemical compositions dominated by calcium and silicon respectively (see below).

The mineralogy of the rock samples was measured at Activation Laboratories, Canada, using a Bruker D8 Endeavour diffractometer equipped with Cu X-ray source measuring at 40 kV and 40 mA over a 4 – 70° range with a step size of 0.02°. The PDF4/Minerals ICDD database was used for mineral identification. The quantities of the crystalline mineral phases were determined by Rietveld refinement of the X-ray diffraction (XRD) patterns. The amounts of the crystalline minerals were recalculated based on a known percent of added corundum and the remainder to 100 % was considered to be comprised of X-ray amorphous and poorly crystalline material. The obtained mineralogical data is reported in Table 4. Note that in this analysis, the clay fraction is reported as the presence or absence of smectite, but is otherwise not quantified.

Table 4 : Mineral composition of the studied rocks as determined by Rietveld refinement of on XRD data (wt%). Note that for smectite, the Y indicates the presence of this phase.

Sample	B83S3	B87S4	B130S2	B261S4	B316S3	HE-65	GOB_14	VP_13	JQ_3-3	KZ_01*	KZ_02*
Amorphous	9.6	29.5	10.4	13.6	20.7	12.4	20.2	10.6	28.9	-	-
Calcite	4	0.7	-	-	-	-	-	-	-	70	-
Dolomite	-	-	-	-	-	-	-	-	-	7	-
Muscovite	-	-	-	-	-	-	-	-	-	23	14
Plagioclase	37.6	5.8	24.9	-	-	33.6	33	60.8	14.4	-	6
K feldspar	-	-	2.7	-	-	-	-	-	-	-	-
Quartz	12	13.6	35.6	37.4	36.6	6.9	-	-	-	-	61
Augite/Diopside	10	10.8	5.3	6	8.6	33	28.5	25.2	26.8	-	-
Pigeonite	-	-	-	-	-	-	7.5	-	2	-	-
Ca Amphibole	-	-	-	-	-	1.6	-	-	-	-	-
Epidote	-	-	-	17.5	28.3	-	-	-	-	-	-
Chlorite	8.1	21.4	6.4	22.7	3.5	7	0.5	n-	-	-	14
Chloritoid	-	-	-	-	-	-	-	-	-	-	5
Smectite*	-	-	-	-	-	Y	Y	Y	-	-	-
Chabazite	-	-	-	-	-	-	0.4	-	-	-	-
Analcime	-	-	-	-	-	-	4.3	-	-	-	-
Clinoptilolite/ Heulandite	-	-	-	-	-	-	-	-	15.9	-	-
Thomsonite	-	-	-	-	-	-	3.5	-	-	-	-
Levyne	-	-	-	-	-	-	0.8	-	7.4	-	-
Laumontite	10.6	15.7	10	0.3	-	-	-	-	-	-	-
Titanite	2.9	2.1	2.7	2.5	2.3	3.9	-	-	0.7	-	-
Ilmenite	-	0.4	-	-	-	-	1.3	1.5	-	-	-
Hematite	4.6	-	1.2	-	-	-	-	-	1.9	-	-
Magnetite	0.6	-	0.8	-	-	1.6	-	1.9	2	-	-

*Mineral composition estimated from the chemical composition and XRD identifications

The amorphous phase content of these rocks is significant, ranging from 9.6 to 29.5%. To investigate the chemical composition this amorphous phase and of the major minerals, thin sections were prepared and analyzed using a CAMECA SXFive electronic microprobe located at the Raimond Castaing micro characterization center in Toulouse. The phases identified using the microprobe are listed in Table S1. The results show the diversity of plagioclases present. The IRDP samples contained plagioclase mostly of albitic composition, while the sample HE-65 and surface rocks contain a mix of labradorite and andesine. The pyroxenes are mainly of augitic composition. The compositions of the amorphous/poorly crystalline fractions

are overall consistent across the samples and are dominated by Al, Fe, Mg and Si (see Figure S1 and Table S2). Compared to basaltic glass, the amorphous/poorly crystalline phase detected in the studied altered basalts had lower Ca and Si contents but higher Fe contents. No consistent trends can be observed in Al and Mg. These compositions are characteristic of altered glass and its transformation into nanocrystalline clay minerals.

2.2. Experimental methods

Mixed flow experiments were conducted in a titanium Parr Reactor system. This system has been previously described by Gudbrandsson et al. (2011) and Marieni et al. (2021). It consists of a 200 ml titanium reactor equipped with a titanium stirring rod driven by an external motor rotating at approximately 250 rpm in this study. A temperature regulator connected to both a heating furnace and an internal thermocouple maintained the temperature of the reactor to 120±2 °C during all experiments. The inlet fluids were stored in compressible polyethylene bags and pumped into the reactor using a Gilson high pressure liquid chromatography (HPLC) pump at rates between 0.27 and 1.95 g/min, leading to a residence time ranging from 103 to 741 min (see Table S3 for the details of each experiment). The residence time is equal to the reactor volume divided by the fluid flow rate. The mechanical steady state in a flow reactor is commonly attained after five residence times, which here ranges from 8 to 25h. The reactor fluid outlet is equipped with an internal 2 μm titanium filter to prevent the original rock powders and/or secondary precipitates from exiting the reactor. A cooling loop protects the stirring mechanism and cools the fluids leaving the reactor from this outlet. A back-pressure regulator, loaded with N_2, maintained the system at approximately 15 bars pressure during all experiments to prevent water boiling.

Before each experiment, the reactor was cleaned and run for at least 24 h at 120 °C with ultrapure water and then with the initial reactive fluid inlet solution. The reactive inlet fluid used in all experiments was made from Merck reagent grade HCl and NaCl diluted into DIW to obtain a pH 3 solution with an ionic strength of 0.01mol·kg^{-1}. This initial reactive fluid pH was selected so that it would have a similar pH to likely CO_2-charged injection waters and to avoid the precipitation of most secondary phases. The pH of water in equilibrium with 25 bars of CO_2 pressure at 25 °C is 3.21 (Gislason et al., 2010). The ionic strength was chosen to mimic the salinity observed in CarbFix injection site (Snæbjörnsdóttir et al., 2017; Clark et al., 2018),

and to facilitate comparison of the results with previously reported data. Fluid samples were regularly collected at the reactor outlet to monitor the reactive fluid flow rate, fluid pH and the concentrations of dissolved major elements. The samples for chemical analyses were immediately acidified with Suprapur HNO_3 and stored prior to elemental analysis.

Most experiments were run until steady-state was attained. Steady-state was assumed when the aqueous silicon concentration of the outlet fluid remained constant within the analytical uncertainty for a period of at least three residence times. At the end of each experiment, the solid fraction was recovered by filtering the reactor's content using a 0.45 µm acetate cellulose filter. The post reaction powders were oven dried at 50 °C for several days and stored for further analyses.

2.3. Reactive fluid and recovered solid analysis

Reactive fluid pH was measured in all outlet samples immediately after sampling using a pH electrode connected to a pH meter (Metrohm). The electrode was calibrated using NIST pH 4.01, 7.00 and 10.01 buffer solutions, and replicate analyses of buffers and samples showed analytical accuracy of 0.03 pH units and precision of ±0.02 pH units at room temperature. Fluid samples were analyzed for Al, Ca, Fe, Mg, and Si concentrations on a Horiba Ultima Expert Inductively Coupled Plasma Optical Emission Spectrometry (ICP-OES) located at Géoscience Environnement Toulouse, with an analytical accuracy better than ±3%, as determined by replicate analyses of certified solutions and samples. The detection limits of these analyses are 5ppb for Al, Ca, Fe, and Mg, but 12ppb for Si. Potassium concentrations were not measured due to its low concentration in the original rocks and in the fluid samples, and Na was not measured as its concentration in the initial reactive aqueous solution was fixed at 0.01 $mol \cdot kg^{-1}$. The powdered samples used in the experiments were analyzed before and after the experiments using XRD and a TESCAN scanning electron microscope (SEM) equipped with an energy dispersive spectrometer (EDS).

2.4. Calculation of saturation states and elemental release rates

The saturation state of the sampled reactive fluids were determined based on the measured fluid elemental concentrations and pH using PHREEQC v 3.6.2 (Parkhurst and Appelo, 2013) together with the CarbFix.dat (V1.1) database (Voigt et al., 2018).

Steady state elemental release rates were calculated using:

(2)

$$r_{i,j} = \frac{C_i * Q}{A_j * m}$$

where $r_{i,j}$ refers to the release rate of the i^{th} element normalized to the surface area A_j, where j represents either BET or geometric surface area. C_i denotes the concentration of the i^{th} element in the outlet fluid, Q designates the flow rate, and m stands for the initial mass of powder introduced into the reactor.

3. RESULTS

3.1. Evolution of the reactive fluid composition

The compositions of all sampled fluids are reported in Table S4 of the supplementary material. The temporal evolution of the pH and measured Si and Ca concentration in all reactive fluids are shown in Figure 3 and Figure 4. Note that the color of the symbols in these figures denotes the type of sample alteration: hydrothermally altered basalts are shown in yellow for zeolites facies alteration samples, in green for epidote facies altered samples, brown for amphibole facies altered samples. Surface weathered samples are depicted in blue and non-basaltic samples are shown with white symbols.

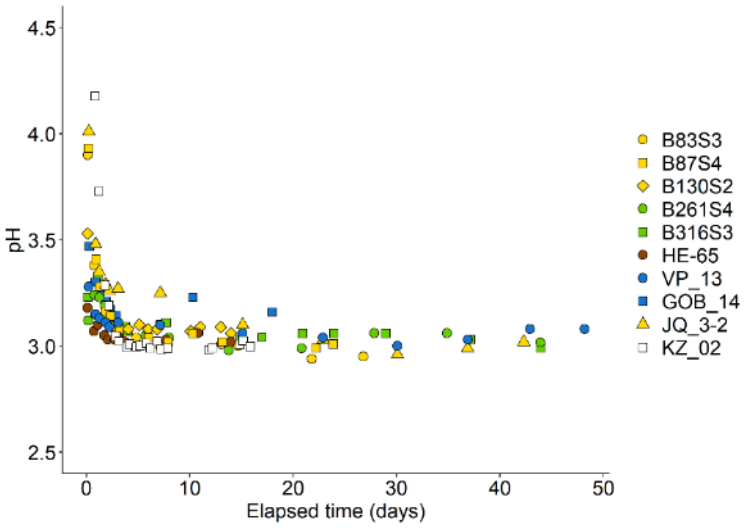

Figure 3 : Temporal pH evolution for all experiments performed in this study. The color of each symbol indicates the type of alteration. Basalts altered at the Earth's surface are shown in blue, rocks altered to the zeolite facies are shown in yellow, basalts altered to the epidote facies are shown in green, basalts altered to the actinolite facies are shown in brown and the non-basalts collected from Turkey, the marble (KZ_01) and the mica schist (KZ_02) are shown in white. Note the pH of the first sample collected from the KZ_02 experiment was 4.86 and that of the samples collected from the KZ_01 are ~6.3 so they do not appear on this figure. The mechanical steady state was reached for all reactors within 25 hours in all experiments.

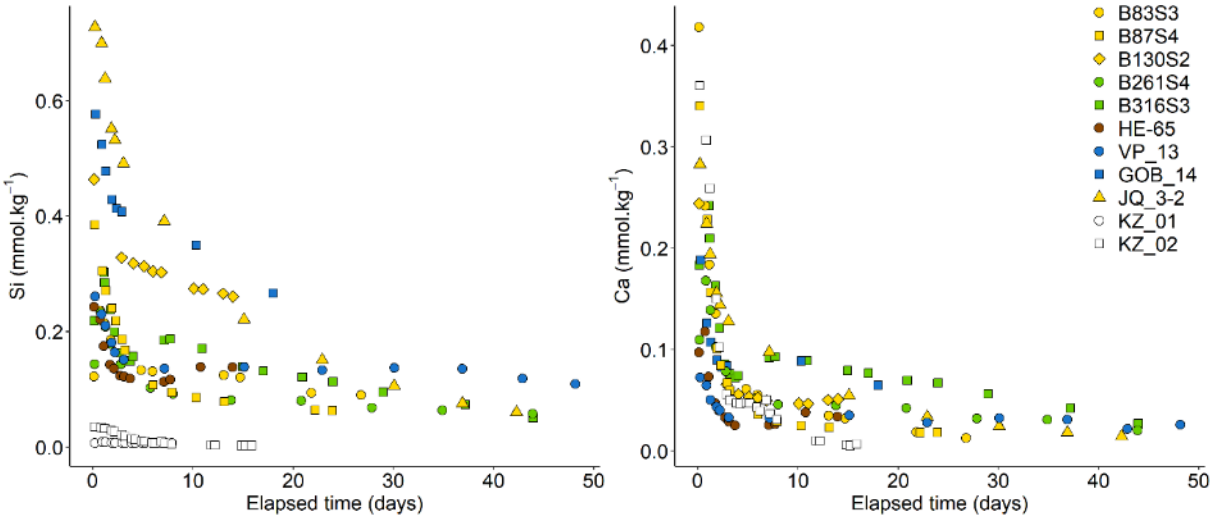

Figure 4 : Temporal evolution of Si (left) and Ca (right) concentrations in the outlet fluids of all experiments in this study. Note the Ca concentrations of experiment KZ_01 are not shown as they are above the maximum value of the plot. See the caption of Fig. 3 for the identity of the color of the symbols.

An initial rapid element release rate is observed for all measured elements during the first 3 days of each experiment. The rapid release coincides with a temporal increase of the pH during this initial period. After this initial phase, the reactive fluid pH decreased to close to its inlet value for all the rock samples, other than KZ_01, and the element release rates progressively stabilized. The maximum measured pH in the reactive fluids was 4.86 for KZ_02 and stayed below pH 4 for all the other experiments, except for sample KZ_01 which remained constant at pH values of ~6.3 due to continuous calcite dissolution. The dissolution of three samples, B83S3, B87S4 and JQ_3-2, attained a pH close to 4 before decreasing back to a pH ~3. For B83S3 and B87S4, the two basalts that contained calcite, mass balance calculations confirmed that the calcite present in these samples was totally dissolved in less than three days for both experiments, such that the longer-term element release rates originate exclusively from the dissolution of the silicate minerals in the dissolving rock samples.

All but three experiments reached steady-state. The dissolution of sample GOB_14 was stopped before steady-state was attained. The fluid Si concentration appears to be decreasing slightly during the end of the B316S3 and JQ_3-2 dissolution experiments. This could be related to the precipitation of secondary phases, partly passivating the reacting mineral surfaces.

It is also worth mentioning that the rock powder formed an aggregate at the bottom of the reactor during dissolution of VP_13. The external part of this aggregate exhibited signs of

extensive reaction, while the inner part appeared preserved. This could lead to an underestimation of the surface area normalized reactivity of this rock. The steady state Ca/Si ratios measured in the outlet fluids as a function of time appear to tend to distinct values as shown in Figure 5 (left).

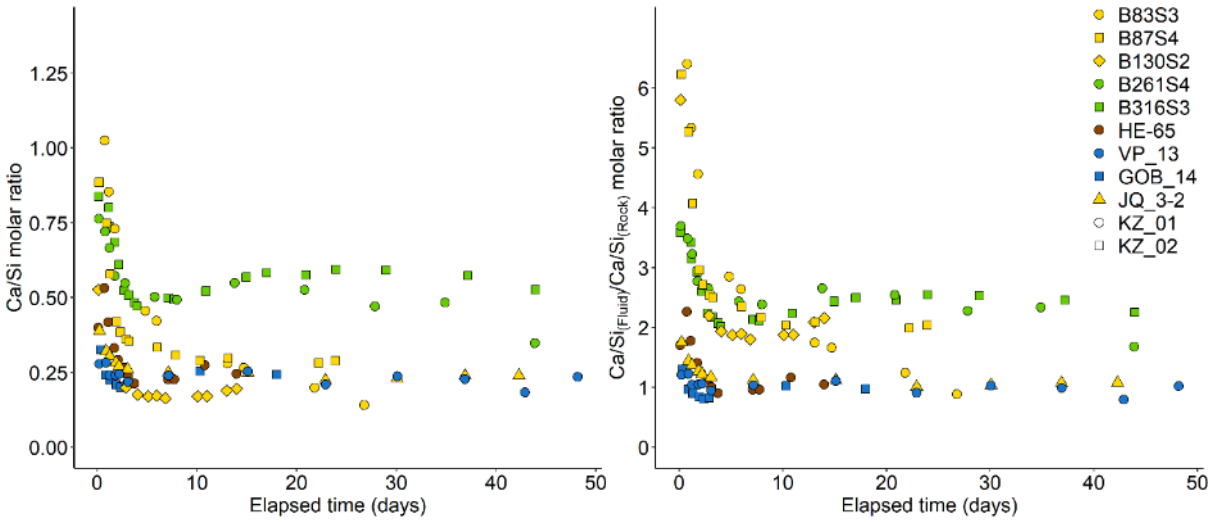

Figure 5 : Temporal evolution of the molar Ca/Si ratio (left) and the molar Ca/Si ratio normalized to that of the rock (right) for each sampled outlet fluid sample of all experiments other than during the KZ_01 and KZ_02 dissolution experiments. The values of these later two experiments lie outside of the plot area due to calcite dissolution and a very low solid sample Ca concentration respectively. See the caption of Fig. 3 for the identity of the color of the symbols.

Two rocks released elements with Ca/Si ratios of approximately 0.5 at steady state, while the other basaltic rock samples released elements with Ca/Si ratios of 0.2 to 0.35. The elemental calcium to silicon ratios of all outlet fluids normalized to the corresponding ratio of the dissolving rock are shown in the right plot of Figure 5. Whereas some of the basaltic rocks rapidly attained a stoichiometric Ca/Si release ratio, others exhibit a preferential release of calcium with a steady state conditions rock normalized molar Ca/Si ratio of approximately 2.

3.2. Saturation states of the reactive fluids and solid alteration products

The calculated saturation states of the sampled outlet fluids with respect to the phases contained in the initial rock samples, as well as potential secondary phases, suggest that some phases are supersaturated and could precipitate. The latter minerals are reported in Table S**5**. The fluids are calculated to be undersaturated with respect to all potential secondary phases except aluminum oxides and hydroxides (all samples) iron oxides (5 samples), and beidellite and kaolinite (4 samples). Several post-experiment powders exhibited a reddish color

indicative of iron oxyhydroxide precipitation. The dissolution of KZ_01 resulted in outlet fluids remaining very close to saturation with calcite throughout the experiment.

Representative SEM images of post-experiment powders are presented in Figure 6. The solids exhibit evident dissolution features, as well as distinctive partial surface coatings consistent with the precipitation of secondary aluminum and iron oxyhydroxide phases. Similar observations were reported by Marieni et al. (2021) when dissolving pure epidote at 100 °C and pH 3.

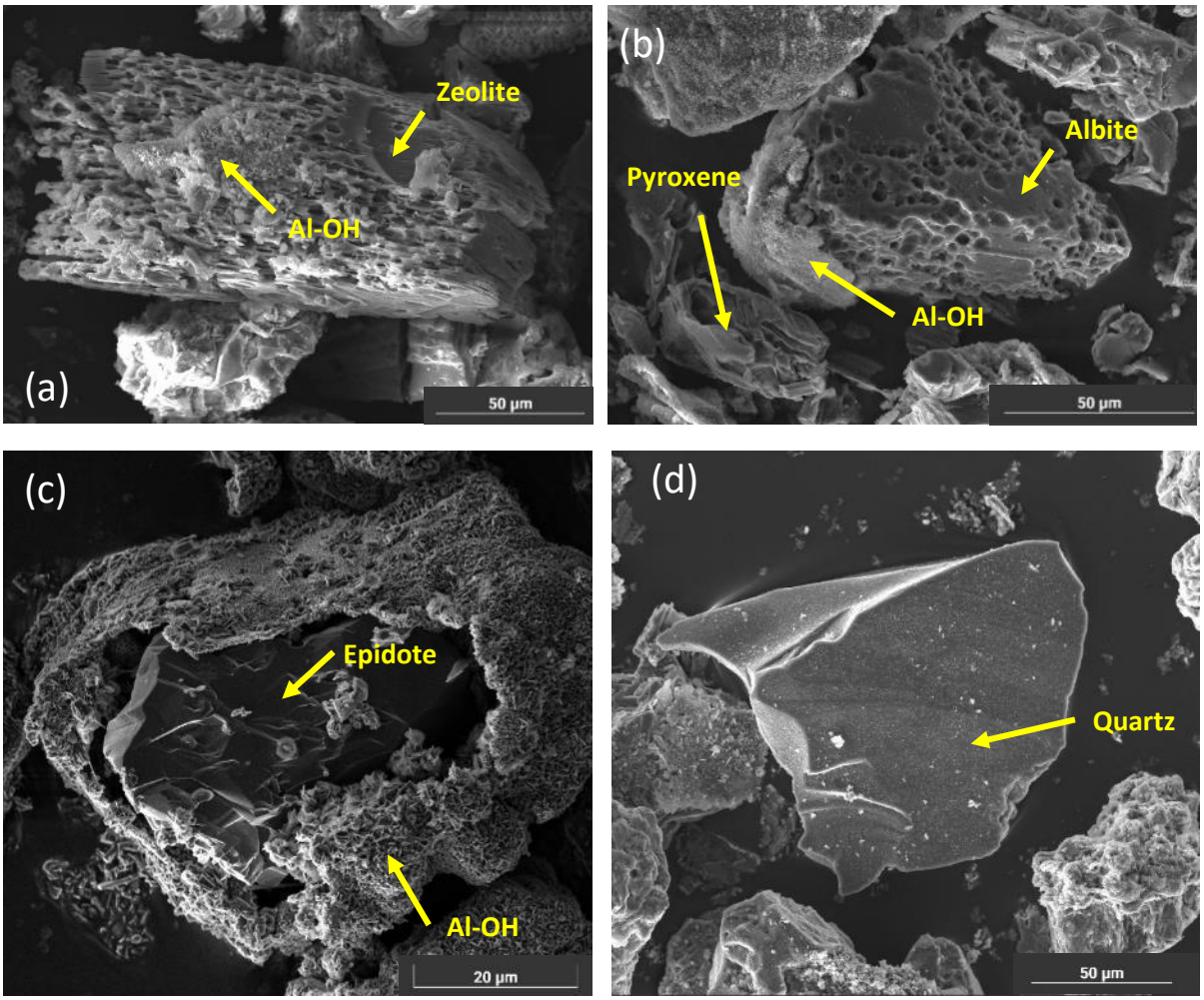

Figure 6 : Representative SEM images of post-experiment powders. (a) A heulandite grain from sample JQ_3-2 showing dissolution features and minor secondary boehmite (Al-OH), (b) a dissolved albite grain from sample GOB_14 partially coated with boehmite, (c) an epidote grain from B316S3 largely coated with boehmite and (d) a quartz grain from B261S4 with neither dissolution feature nor coatings.

The XRD analyses of the post reaction powders confirmed the precipitation of boehmite in samples B261S4, B316S3, GOB_14, VP_13, and JQ_3-2. Iron oxyhydroxides were not detected using XRD. Based on the relative amplitude of the peaks before and after reaction, the XRD

results indicate the total dissolution of calcite, the significant dissolution of zeolites, epidote, and chlorite, and partial dissolution of plagioclase and pyroxenes, magnetite, titanite from the basaltic samples. These observations suggest the preferential dissolution of zeolites over plagioclases, and of epidote over quartz in the more altered rocks.

3.3. Element Release rates

Silicon release rates are commonly used to quantify silicate mineral dissolution rates. This choice stems from the role of silicon in maintaining the crystalline structure of these minerals. Steady-state silicon release rates of all rock samples calculated from equation (2) and based on BET and geometric surface areas are listed in Table 5 and plotted in Figure 7.

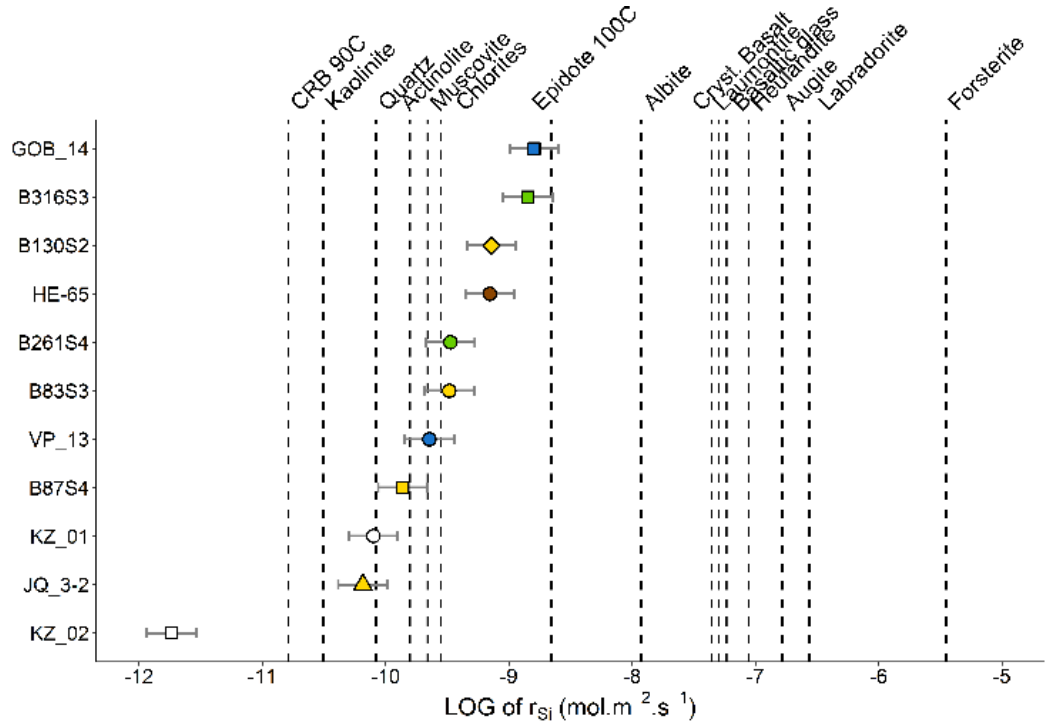

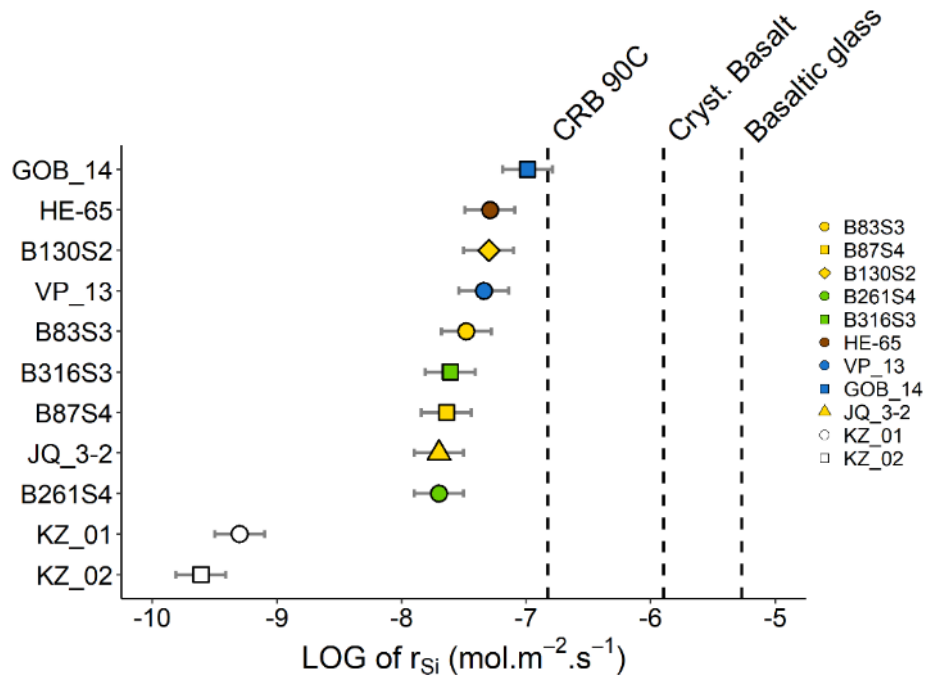

Figure 7 : Logarithm of measured silicon release rates normalized to BET (upper plot) and geometric (lower plot) surface area together with those of various single minerals calculated using equations reported by Heřmanská et al. (2022) *or of rocks. CRB 90C stands for a Columbia River Basalt dissolved at 90 °C* (Schaef and McGrail, 2009)*. Epidote 100C refers to rates of Si release from epidote at 100 °C (Marieni et al., 2021). Crystalline basalt's rates were reported by Gudbrandsson et al. (2011). Basaltic glass rates were reported by Gislason and Oelkers (2003). The uncertainty on the measured values is depicted with error bars. See the caption of Fig. 3 for the identity of the color of the symbols.*

The logarithm of silicon release rates normalized to BET surface area and in units of mol·m^{-2}·s^{-1} measured on all samples varied between -10.18 and -8.80 except for sample KZ_02, which had a value of -11.74 (Figure 7). Silicon release rates from all the studied altered basalts are within one and a half order of magnitude of each other and fall in a range close to previously reported dissolution rates of diopside, epidote, quartz and actinolite. The logarithm of dissolution rates of reference minerals and rocks such as basaltic glass and fresh crystalline basalt are also displayed for comparison. The measured BET normalized element release rates in this study are two to three orders of magnitude slower than those of the basaltic glass and the fresh crystalline basalt. Compared to the rates measured in this study, the Si release rates of Columbia River Basalt at 90 °C normalized to BET surface area reported by Schaef et al. (2009) are slower whereas their geometric surface normalized rates are faster. The logarithm of Si release rates normalized to geometric surface area measured in this study are within one order of magnitude of each other, ranging between -7.70 and -6.99 except for the non-basaltic samples, KZ_01 and KZ_02 which had logarithm of Si release rates equal to -9.30 and -9.61, respectively (lower Figure 7, Table 5).

Table 5 : Logarithm of the BET and geometric surfaces area normalized rates in units of mol·m^{-2}·s^{-1} for all samples.

	log rate (mol·m^{-2}·s^{-1})							
SAMPLE	**Si_{BET}**	**Si_{GEO}**	**Ca_{BET}**	**Ca_{GEO}**	**Mg_{BET}**	**Mg_{GEO}**	**Fe_{BET}**	**Fe_{GEO}**
B83S3	-9.48	-7.48	-10.16	-8.16	-10.36	-8.35	-10.68	-8.67
B87S4	-9.86	-7.64	-10.40	-8.17	-10.68	-8.45	-10.88	-8.65
B130S2	-9.14	-7.30	-9.87	-8.03	-10.59	-8.75	-10.79	-8.95
B261S4	-9.47	-7.70	-9.75	-7.98	-10.14	-8.36	-10.35	-8.57
B316S3	-8.85	-7.61	-9.09	-7.86	-9.82	-8.59	-9.97	-8.73
HE-65	-9.15	-7.29	-9.75	-7.89	-10.15	-8.29	-10.25	-8.39
GOB_14	-8.80	-6.99	-9.40	-7.59	-9.43	-7.62	-9.82	-8.01
JQ_3-2	-10.18	-7.70	-10.80	-8.33	-10.94	-8.46	-11.48	-9.00
VP_13	-9.65	-7.34	-10.29	-7.99	-10.50	-8.20	-10.89	-8.59
KZ_01	-10.10	-9.30	-8.03	-7.23	-9.03	-8.24	<QL	<QL
KZ_02	-11.74	-9.61	-11.44	-9.32	<QL	<QL	-12.46	-10.33

<QL denotes values below the quantification limit of the ICP-OES analysis

The measured steady-state release rates of calcium, magnesium and iron, three cations that potentially promote carbon mineralization, are listed in Table 5 and plotted in Figure 8 for Ca and Mg, and in figure S2 for Fe.

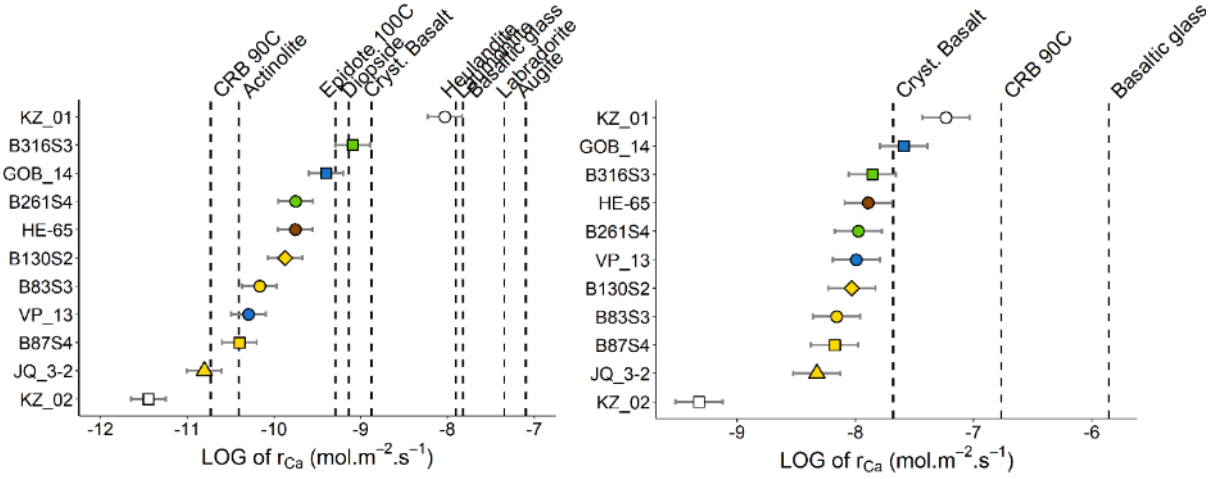

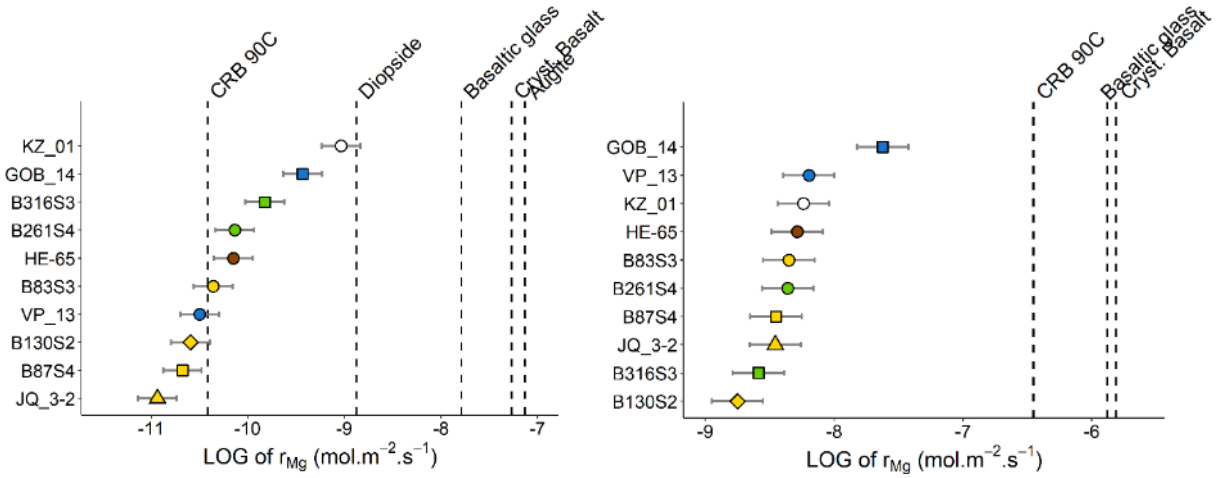

Figure 8 : Logarithms of the calcium (upper), and magnesium (lower) release rates normalized to BET (left) and geometric (right) surface areas respectively in units of mol·m^{-2}·s^{-1} measured in this study. The sources of the rates of minerals, and rocks are provided in the caption of Fig. 7. The uncertainty on the measured values is depicted with error bars. See the caption of Fig. 3 for the identity of the color of the symbols.

The measured BET normalized element release rates of the basaltic rocks in units of mol·m^{-2}·s^{-1} range from -10.80 to -9.09 for calcium and from -10.94 to -9.43 for magnesium. The logarithm of the element release rates for the two non-basaltic rocks, KZ_01 and KZ_02 were -8.03 and -11.44 for calcium and -9.03 and not measurable for magnesium, respectively. The geometric surface areas normalized calcium and magnesium release rates were within one order of magnitude of each other for the altered basaltic rocks, and approximately two orders of magnitude faster than corresponding BET normalized rates.

The largest contribution to the uncertainty in the measured elemental release rates likely stems from the uncertainties in the measured surface areas. Other contributions to uncertainty include the measurement of element concentrations in the fluid and solid phases, and the fluid flow rate. Taken together these factors suggest a measurement uncertainty of approximately ±0.2 log units. Nevertheless there appears to be far more scatter among experimentally measured mineral dissolution rates reported for distinct samples (Palandri and Kharaka, 2004; Brantley, 2008; Schott et al., 2009; Heřmanská et al., 2022). Such comparisons suggest that the reproducibility of surface area normalized measured elemental release rates among distinct rock or mineral samples may be on the order of ±0.5 log units or more.

4. Discussion

4.1. Evolution of the release of major elements

During the first part of each experiment, the element release rates exhibit two distinct features: 1) the relatively fast release of Si compared to the later parts of the experiment and 2) the preferential release of Ca and Mg compared to Si. This former observation could be attributed to the rapid dissolution of fine particles or high energy surfaces created by particle preparation and/or minor (highly reactive) phases of high surface area. Note, however, that few fine particles were observed by SEM in the initial powders. For some samples, this increased Si release is sustained for longer, up to 20 days after the beginning of the reaction, and could be attributed to the dissolution of highly reactive phases such as zeolites, up to their exhaustion as for Heulandite and Levyne in the case of JQ_3-2. Indeed, those phases were no longer detected in the post reaction powder. The initial preferential release of Ca and Mg that occurred in the first day of each experiment could be attributed, except for samples with calcite, to proton exchange for interlayer Ca in clays and/or Ca at or near the mineral surfaces (Oelkers et al., 1994, 2009; Oelkers and Gislason, 2001; Oelkers and Schott, 2001). This possibility is supported by the concurrent increase in pH observed during the initial part of each dissolution experiment. After this initial period, the release rates and the Ca and Mg ratios to Si reached their steady state values.

The relative element release rates at steady-state provide insight into the whole rock dissolution process. Numerous rocks exhibit steady-state Ca/Si release ratios close to that of the corresponding rock including the surface altered basalts and the rock sample collected from the Hellisheiði core, whose compositions are dominated by plagioclase and pyroxenes. In contrast, a second group of rocks exhibit a long-term preferential release of Ca. This second group consists of the more altered rocks containing substantial zeolite and epidote. This long-term preferential release of Ca suggests that these Ca bearing silicates dissolve more rapidly than the Ca-free silicates in these rocks. Some of this observed long-term preferential Ca release from the most altered basalts is due to the presence of relatively unreactive Si rich, Ca poor phases, such as quartz and chlorites. But the relatively fast dissolution rate of secondary Ca bearing minerals also contributes to this preferential Ca release. Ragnarsdóttir (1993) showed that the zeolite heulandite has dissolution rates of approximately $10^{-9.7}$ mol·m^{-2}·s^{-1} at pH ~3 and 25 °C and pointed the similarity in rates between heulandite and laumontite. At 120 °C, these dissolution rates are likely on the order of 10^{-8}, which is similar to that of basaltic glass. The preferential dissolution of zeolites in the experiments was also confirmed by the

XRD analyses of post reaction powders. Similarly, the relatively high Ca/Si release rates for samples B261S4 and B316S3 can be attributed to the presence of epidote in these rocks. The Ca/Si element release ratio during the dissolution of these rocks trended towards 0.5, which is close to the 0.66 Ca/Si atomic ratio of epidote. In the case of the calcite bearing altered basalts, samples B83S3 and B87S4, the initial solid Ca/Si ratios do not correspond to that in the reactor fluid at steady-state, since the calcite in these rocks was completely dissolved during the first few days of their dissolution experiments. The Ca/Si ratios of these rocks, however, after the removal of calcite are 0.11 and 0.13 for samples B83S3 and B87S4, respectively. The Ca/Si release ratios measured in the fluids normalized to the corresponding calcite free rock compositions of these rocks are 1.90 and 2.23, respectively, indicating the preferential release of calcium from the silicate minerals in these altered basalts as well. In contrast, the Mg/Si ratios of the outlet fluids were closer to those of the corresponding dissolving basalt.

4.2. Processes controlling the release rates of the individual elements

There are several notable observations among the release rates of the elements from the studied altered basalts. First, the release rates of each element are similar for all the altered basalts despite the varying degree of basalt alteration. A similar observation was reported by Nesbitt and Wilson (1992) who observed that the bulk leach rates of the major elements from weathered basalts are not greatly affected by the mineralogy or bulk composition of the parent basalt. Indeed, all the basaltic samples dissolved in the present study exhibit silicon release rates within less than 1.5 orders of magnitudes of each other when normalized to BET surface area and within 0.6 orders of magnitude when normalized to geometric surface area. The similarity of the silicon release rates in the altered basalts can be attributed to the similar dissolution rates of the some of the phases present in the rocks. The natural alteration of basalts rapidly removes the most reactive phases such as basaltic glass, olivine, and anorthitic feldspar. The BET surface area normalized dissolution rates at pH 3, 120 °C dissolution rates of many of the phases remaining in the altered basalts including the pyroxenes, albitic plagioclase, the zeolite minerals and epidote are all within two orders of magnitude of each other. In contrast, the dissolution rates of chlorite, the clay minerals and quartz are far lower and likely contribute negligibly to the overall release of elements from the dissolving basalts.

A second notable observation is that the Ca and Mg release rates of the altered basalts are close to one another when normalized to the geometric surface area. During the alteration process, Ca is mostly relocated into zeolites or epidote whereas Mg is mostly precipitated into clays and chlorites. These sheet silicate minerals have dissolution rates that are orders of magnitude slower than those of basaltic glass, olivine, zeolites and pyroxene (see Figure 7 upper). But the persistence of pyroxene in all of the altered basalt samples permits the continued release of Mg to solution despite the extensive alteration of some of the basalt samples. In the case of olivine bearing rocks such as crystalline basalt, the drop in Mg release rates from fresh to altered rock is far more than the Ca release rates. This observation stems largely from the removal of olivine and to a lesser extent basaltic glass from these rocks and the relocation of Mg into slower dissolving phases such as smectite and chlorite. In contrast, the Ca released from the dissolution of basaltic glass or anorthite plagioclase reactions is mostly precipitated into zeolites or epidote, which have similar dissolution rates as the dissolving primary Ca bearing silicates in fresh basalt.

4.3. Surface area and element release rates

The application water-mineral or water-rock reaction rates measured in the laboratory to field conditions commonly relies on the normalization of rates to the solid-fluid interfacial surface area. The results of this study highlight some of the challenges of normalizing dissolution rates of natural rocks to their surface area. Despite all the samples being prepared in the same laboratory using the same methods, the observed BET/GEO ratios of the rocks considered in this study range from 14 to 301. Some of this variation may be due to the presence of remaining ultrafine particles that were not detected on the SEM. It seems likely however, that much of the variation of the BET/GEO ratio, stems from the high surface areas of some of the major secondary phases formed during basalt alteration, notably chlorite, zeolite, and clay minerals. Chlorite, zeolite (Yates, 1968; Valdés et al., 2006) and clay (Murray and Quirk, 1990) minerals have been reported to exhibit elevated surface roughness factors. In addition, Brantley and Mellott, (2000) reported the presence of substantial ‘internal porosity’ in chlorite, zeolite and clay minerals .

The role of mineralogy in influencing measured rock surface areas is also evident in the results of the present study. For example, the BET/GEO surface area ratios of the shallower IRDP

samples, which contain zeolite, are two to ten times higher than those of B216S4 and B316S3, which do not contain zeolites.

Large differences in the BET/GEO surface area ratios of samples, such as measured in this study, renders the comparison of surface area normalized element release rates of rocks having distinct compositions to be somewhat ambiguous. The observation that distinct minerals and surfaces react at distinct rates (e.g. Sanders et al., 2010) adds to such ambiguities. This issue is evident in the study of Schaef and McGrail, (2009), who reported that the dissolution rates of Columbia river basalts were more than 1000 times higher when normalized to the calculated geometric surface area compared to those normalized to the measured BET surface area. This basalt was reported to be almost as reactive as basaltic glass when comparing geometric surface area normalized rates, whereas, these rates were approximately 3 orders of magnitude slower than the corresponding rates of basaltic glass when normalized to their BET surface area. Such ambiguities hamper the comparison of measured rates and lead to substantial uncertainties when applying element release rates measured in the laboratory to field applications.

The consequences of the elevated BET surface areas of some rocks due to secondary phases are evident in the results of the present study. For example, both B130S2 and JQ_3-2 are altered to the zeolites facies, with plagioclase, pyroxenes and zeolites being the most reactive phases. However, JQ_3-2 having a BET surface area more than four times that of B130S2, the former exhibits release rates consistently lower than the latter. The same is observed when comparing the two samples altered to the epidote facies, B216S4 and B316S3 which have very similar mineralogy, but B216S4's BET surface area is more than three times that of B316S3. As a result, B261S4 appears consistently less reactive than B316S3 when normalized to BET surface area. The inflated BET surface areas of these samples thus lead to underestimate their dissolution rates normalized to the BET surface area. This contrast suggests that much of the additional BET surface area created by the alteration of basalts is relatively unreactive, and illustrates the potential ambiguity when applying BET surface areas for the normalization of release rates from natural rocks whose constituting minerals cover a very large spectrum of surface areas.

4.4. The role of secondary phases in mineral carbonation

The observation that highly altered basalts with only minor remaining primary phases are able to sustain substantial divalent metal release rates suggests that some of the secondary phases can help promote mineral carbonation. Notably calcium bearing zeolites have a Ca to Si ratio and dissolution rates comparable to plagioclase (Ragnarsdóttir, 1993; Savage et al., 1993). The initial release of Ca to the fluid during zeolite dissolution may be enhanced by its non-stochiometric dissolution as reported by Hartman and Fogler (2007). In the case of epidote, although its dissolution rates are somewhat slower than that of plagioclase, its calcium to Si ratio content is more than twice as great as that of the major zeolites. This mineral has also been observed to preferentially release Ca from its structure during its dissolution (Marieni et al., 2021). Other secondary phases present in the altered basalts, however may contribute relatively little to mineral carbonation. The amorphous phases present in the altered samples are largely depleted in calcium partly depleted in silicon and enriched in iron compared to basaltic glass. The presence of this altered amorphous phase did not result in a higher reactivity of the altered rocks, suggesting that it is relatively unreactive and would contribute less than primary or some secondary Ca bearing crystalline silicates to mineral carbonation. In contrast to Ca, the Mg secondary phases, dominated by chlorite and clay minerals are relatively unreactive. The release of Mg from altered basalts is likely maintained by the continued presence of pyroxenes in the altered basalts.

Equally, the minerals present in the non-basaltic samples considered in this study, KZ_01 and KZ-02 will also likely to contribute negligibly to mineral carbonation. These rocks exhibit geometrically surface area normalized Si release rates that are 1 to 1.5 orders of magnitude lower than those of the altered basalts and similar BET surface area normalized Si release rates to quartz and kaolinite. The Ca and Mg released from sample KZ-01 largely originated from the dissolution of carbonate minerals, such that the carbonation of these elements would lead to no net carbon mineral storage in the subsurface. The rate of Ca release from the mica schist, KZ_02, is far slower than that of the altered basalts and the rate of Mg release from this rock was below the detection limit of the experiments despite the presence of substantial chlorite in the rock. These observations illustrate the relatively large potential of altered basalt carbonation compared to these common meta-sedimentary rocks.

4.5. Implications for subsurface CO_2 mineral storage

Rock dissolution and the release of divalent metals to aqueous solution are one of the rate limiting steps of the carbon mineralization process (Oelkers et al., 2008; Gadikota et al., 2020). The original CarbFix injection successfully mineralized 95% of the CO_2 injected into relatively fresh basalts at a temperature of ~20 to 33 °C within two years (Matter et al., 2016). The findings of the present study suggest that the dissolution rates of altered basalts are approximately independent of their degree of alteration and that they dissolve approximately 2 orders of magnitude slower than corresponding basaltic glass or olivine bearing fresh crystalline basalt. This observation suggests that the carbonation of altered basalt would take approximately 100 times longer than the carbonation of fresh basalt. As such, one might expect that the carbonation of subsurface altered basalts in similar conditions (~33 °C) would require ~200 years. Mineral dissolution rates, however, increase substantially with increasing temperature. The dissolution rates of most major silicate minerals increase by approximately two orders of magnitude when increasing temperature from 30 to 100 °C at acidic conditions (Casey and Sposito, 1992; Oelkers, 2001; Heřmanská et al., 2022). Indeed, the element release rates determined in the present study at 120 °C are similar to those of basaltic glass and olivine bearing fresh crystalline basalt at 25 °C. It therefore seems likely that the carbonation of altered basalts at temperatures of ~100 °C or higher could be as rapid as that of the original CarbFix injection. Such conditions are readily found in geothermal systems (Wu and Li, 2020). This conclusion is supported by the sequestration of carbon through mineralization reactions during the ongoing CarbFix2 injections, where more than half of the CO_2 injected into altered basalts at temperature of ~250 °C was mineralized within four months (Clark et al., 2020).

5. Conclusions

All of the altered basalts considered in this study have been observed to dissolve and release their Si, Ca, and Mg to the fluid phase at rates from one to three orders of magnitude slower than corresponding fresh crystalline basalt or basaltic glass depending on the element and surface area used to normalize rates. The element release rates from these rocks are close to independent of the degree of alteration of the basalts. This observation has been attributed to the fact that the alteration process removes the most reactive phases such as basaltic glass and olivine, and that the remaining primary silicate minerals, plagioclase and pyroxenes, and

many of the secondary phases, notably zeolites and epidote, have dissolution rates that differ by less than two orders of magnitude from each other.

The observation that altered basalts readily release Si, Ca, and Mg to the fluid attest to their ability to react with dissolved CO_2 as part of mineral carbon storage efforts. Although the element release rates are 1 to 3 orders of magnitude slower than that of unaltered basalts, mineral dissolution rates increase substantially with increasing temperature. The element release rates from altered basalts observed in this study at 120 °C approximate the element release rates of basaltic glass and olivine at ambient temperatures. As the original CarbFix project demonstrated the successful carbonation of more than 95% of the CO_2 injected into fresh basalts as a water dissolved phase at near to ambient temperatures, it can be anticipated that the carbonation of altered basalts could be equally fast and effective at temperatures at or above 100 °C. At lower temperatures, it seems likely that mineral carbonation would be favorable, but at a slower rate.

Such observations encourage the storage of CO_2 via mineral storage into the vast quantities of altered basalts that are available worldwide, both on the continents and offshore. The results obtain in this study particularly points towards attempting carbon storage into geothermal areas where higher temperature gradients are available. Parts of the geothermal fields where the temperature may not be high enough for energy production could prove useful for in situ mineralization in altered basalts.

6. Acknowledgments

The authors are particularly grateful to Matylda Heřmanská and Iwona Galeczka for their help in sampling during COVID lockdowns with the valuable advice of Birgir Vilhelm Óskarsson. They also thank Sigurdur R. Gislason for coordinating access to the IRDP core. The authors acknowledge the valuable insights and support from Chiara Marieni, Giuseppe Saldi, Carole Causserand, Alain Castillo and Pascal Gisquet.

7. Funding

This work has been carried out within the European projects CarbFix2 and GECO that have received funding from the European Union's Horizon 2020 research and innovation program under grant agreements No 764760 and number 818169, respectively.

8. References

Adeoye, J.T., Menefee, A.H., Xiong, W., Wells, R.K., Skemer, P., Giammar, D.E., Ellis, B.R., 2017. Effect of transport limitations and fluid properties on reaction products in fractures of unaltered and serpentinized basalt exposed to high PCO_2 fluids. Int. J. Greenh. Gas Control 63, 310–320. https://doi.org/10.1016/j.ijggc.2017.06.003

Berger, G., Cadore, E., Schott, J., Dove, P.M., 1994. Dissolution rate of quartz in lead and sodium electrolyte solutions between 25 and 300°C: Effect of the nature of surface complexes and reaction affinity. Geochim. Cosmochim. Acta 58, 541–551. https://doi.org/10.1016/0016-7037(94)90487-1

Berner, R.A., 2004. The Phanerozoic Carbon Cycle, OUP E-Books. Oxford University Press. https://doi.org/10.1093/oso/9780195173338.001.0001

Berner, R.A., Lasaga, A.C., Garrels, R.M., 1983. The carbonate-silicate geochemical cycle and its effect on atmospheric carbon dioxide over the past 100 million years. Am. J. Sci. 283, 641–683. https://doi.org/10.2475/ajs.283.7.641

Brady, P. V., Carroll, S.A., 1994. Direct effects of CO_2 and temperature on silicate weathering: Possible implications for climate control. Geochim. Cosmochim. Acta 58, 1853–1856. https://doi.org/10.1016/0016-7037(94)90543-6

Brady, P. V., Walther, J. V., 1990. Kinetics of quartz dissolution at low temperatures. Chem. Geol. 82, 253–264. https://doi.org/10.1016/0009-2541(90)90084-K

Brantley, S.L., 2008. Kinetics of Mineral Dissolution, in: Kinetics of Water-Rock Interaction. Springer, New York, NY, p. 833. https://doi.org/https://doi.org/10.1007/978-0-387-73563-4_5

Brantley, S.L., Mellott, N.P., 2000. Surface area and porosity of primary silicate minerals. Am. Mineral. 85, 1767–1783. https://doi.org/10.2138/am-2000-11-1220

Casey, W.H., Sposito, G., 1992. On the temperature dependence of mineral dissolution rates. Geochim. Cosmochim. Acta 56, 3825–3830. https://doi.org/10.1016/0016-7037(92)90173-G

Chukwuma, J.S., Pullin, H., Renforth, P., 2021. Assessing the carbon capture capacity of South Wales' legacy iron and steel slag. Miner. Eng. 173, 107232. https://doi.org/10.1016/j.mineng.2021.107232

Clark, D.E., Gunnarsson, I., Aradóttir, E.S., Þ. Arnarson, M., Þorgeirsson, Þ.A., Sigurðardóttir, S.S., Sigfússon, B., Snæbjörnsdóttir, S.Ó., Oelkers, E.H., Gíslason, S.R., 2018. The chemistry and potential reactivity of the CO2 -H2S charged injected waters at the basaltic CarbFix2 site, Iceland. Energy Procedia 146, 121–128. https://doi.org/10.1016/j.egypro.2018.07.016

Clark, D.E., Oelkers, E.H., Gunnarsson, I., Sigfússon, B., Snæbjörnsdóttir, S., Aradóttir, E.S., Gíslason, S.R., 2020. CarbFix2: CO_2 and H_2S mineralization during 3.5 years of continuous injection into basaltic rocks at more than 250 °C. Geochim. Cosmochim. Acta 279, 45–66. https://doi.org/10.1016/j.gca.2020.03.039

Critelli, T., Marini, L., Schott, J., Mavromatis, V., Apollaro, C., Rinder, T., De Rosa, R., Oelkers, E.H., 2014. Dissolution rates of actinolite and chlorite from a whole-rock experimental study of metabasalt dissolution from 2≤pH≤12 at 25°C. Chem. Geol. 390, 100–108. https://doi.org/10.1016/j.chemgeo.2014.10.013

Fridleifsson, I.B., Gibson, I.L., Hall, J.M., Johnson, H.P., Chistensen, N.I., Schmincke, H.-U., Schönharting, G., 1982. The Iceland Research Drilling Project. J. Geophys. Res. 87, 6359–6361. https://doi.org/10.1029/JB087iB08p06359

Fuhr, M., Geilert, S., Schmidt, M., Liebetrau, V., Vogt, C., Ledwig, B., Wallmann, K., 2022. Kinetics of Olivine Weathering in Seawater: An Experimental Study. Front. Clim. 4, 1–20. https://doi.org/10.3389/fclim.2022.831587

Gadikota, G., Matter, J., Kelemen, P., Brady, P. V., Park, A.H.A., 2020. Elucidating the differences in the carbon mineralization behaviors of calcium and magnesium bearing alumino-silicates and magnesium silicates for CO2 storage. Fuel 277, 117900. https://doi.org/10.1016/j.fuel.2020.117900

Gaillardet, J., Dupré, B., Louvat, P., Allègre, C.J., 1999. Global silicate weathering and CO_2 consumption rates deduced from the chemistry of large rivers. Chem. Geol. 159, 3–30. https://doi.org/10.1016/S0009-2541(99)00031-5

Galeczka, I.M., Stefánsson, A., Kleine, B.I., Gunnarsson-Robin, J., Snæbjörnsdóttir, S.Ó., Sigfússon, B., Gunnarsdóttir, S.H., Weisenberger, T.B., Oelkers, E.H., 2022. A pre-injection assessment of CO_2 and H_2S mineralization reactions at the Nesjavellir (Iceland) geothermal storage site. Int. J. Greenh. Gas Control 115. https://doi.org/10.1016/j.ijggc.2022.103610

Gautier, J.M., Oelkers, E.H., Schott, J., 2001. Are quartz dissolution rates proportional to B.E.T. surface areas? Geochim. Cosmochim. Acta 65, 1059–1070. https://doi.org/10.1016/S0016-7037(00)00570-6

Gislason, S.R., Oelkers, E.H., 2003. Mechanism, rates, and consequences of basaltic glass dissolution: II. An experimental study of the dissolution rates of basaltic glass as a function of pH and temperature. Geochim. Cosmochim. Acta 67, 3817–3832. https://doi.org/10.1016/S0016-7037(00)00176-5

Gislason, S.R., Oelkers, E.H., Eiriksdottir, E.S., Kardjilov, M.I., Gisladottir, G., Sigfusson, B., Snorrason, A., Elefsen, S., Hardardottir, J., Torssander, P., Oskarsson, N., 2009. Direct evidence of the feedback between climate and weathering. Earth Planet. Sci. Lett. 277, 213–222. https://doi.org/10.1016/j.epsl.2008.10.018

Gislason, S.R., Sigurdardóttir, H., Aradóttir, E.S., Oelkers, E.H., 2018. A brief history of CarbFix: Challenges and victories of the project's pilot phase. Energy Procedia 146, 103–114. https://doi.org/10.1016/j.egypro.2018.07.014

Gudbrandsson, S., Wolff-Boenisch, D., Gislason, S.R., Oelkers, E.H., 2011. An experimental study of crystalline basalt dissolution from 2≤pH≤11 and temperatures from 5 to 75°C. Geochim. Cosmochim. Acta 75, 5496–5509. https://doi.org/10.1016/j.gca.2011.06.035

Gunnarsson, I., Aradóttir, E.S., Oelkers, E.H., Clark, D.E., Þór, M., Sigfússon, B., Snæbjörnsdóttir, S.Ó., Matter, J.M., Stute, M., Júlíusson, B.M., Gíslason, S.R., 2018. The rapid and cost-effective capture and subsurface mineral storage of carbon and sulfur at the CarbFix2 site. Int. J. Greenh. Gas Control 79, 117–126. https://doi.org/10.1016/j.ijggc.2018.08.014

Gustafsson, Å.B., Puigdomenech, I., 2003. The effect of pH on chlorite dissolution rates at 25°C. Mater. Res. Soc. Symp. - Proc. 757, 649–655. https://doi.org/10.1557/proc-757-ii3.16

Harrison, A.L., Power, I.M., Dipple, G.M., 2013. Accelerated carbonation of brucite in mine tailings for carbon sequestration. Environ. Sci. Technol. 47, 126–134. https://doi.org/10.1021/es3012854

Hartman, R.L., Fogler, H.S., 2007. Understanding the dissolution of zeolites. Langmuir 23, 5477–5484. https://doi.org/10.1021/la063699g

Hartman, R.L., Fogler, H.S., 2005. Reaction Kinetics and Mechanisms of Zeolite Dissolution in Hydrochloric Acid. Ind. Eng. Chem. Res. 44, 7738–7745. https://doi.org/10.1021/ie0504349

Heřmanská, M., Voigt, M.J., Marieni, C., Declercq, J., Oelkers, E.H., 2022. A comprehensive and internally consistent mineral dissolution rate database: Part I: Primary silicate minerals and glasses. Chem. Geol. 597. https://doi.org/10.1016/j.chemgeo.2022.120807

House, W.A., Orr, D.R., 1992. Investigation of the pH dependence of the kinetics of quartz dissolution at 25°C. J. Chem. Soc. Faraday Trans. 88, 233–241. https://doi.org/10.1039/FT9928800233

Huijgen, W.J.J., Witkamp, G.J., Comans, R.N.J., 2005. Mineral CO_2 sequestration by steel slag carbonation. Environ. Sci. Technol. 39, 9676–9682. https://doi.org/10.1021/es050795f

Kalinowski, B.E., Faith-Eii, C., Schweda, P., 1998. Dissolution kinetics and alteration of epidote in acidic solutions at 25°C. Chem. Geol. 151, 181–197. https://doi.org/10.1016/S0009-2541(98)00079-5

Kantola, I.B., Masters, M.D., Beerling, D.J., Long, S.P., DeLucia, E.H., 2017. Potential of global croplands and bioenergy crops for climate change mitigation through deployment for enhanced weathering. Biol. Lett. 13. https://doi.org/10.1098/rsbl.2016.0714

Kelemen, P.B., Aines, R., Bennett, E., Benson, S.M., Carter, E., Coggon, J.A., de Obeso, J.C., Evans, O., Gadikota, G., Dipple, G.M., Godard, M., Harris, M., Higgins, J.A., Johnson, K.T.M., Kourim, F., Lafay, R., Lambart, S., Manning, C.E., Matter, J.M., Michibayashi, K., Morishita, T., Noël, J., Okazaki, K., Renforth, P., Robinson, B., Savage, H., Skarbek, R., Spiegelman, M.W., Takazawa, E., Teagle, D., Urai, J.L., Wilcox, J., 2018. In situ carbon mineralization in ultramafic rocks: Natural processes and possible engineered methods. Energy Procedia 146, 92–102. https://doi.org/10.1016/J.EGYPRO.2018.07.013

Kelemen, P.B., Matter, J., 2008. In situ carbonation of peridotite for CO_2 storage. Proc. Natl. Acad. Sci. 105, 17295–17300. https://doi.org/10.1073/pnas.0805794105

Kelemen, P.B., Matter, J., Streit, E.E., Rudge, J.F., Curry, W.B., Blusztajn, J., 2011. Rates and Mechanisms of Mineral Carbonation in Peridotite: Natural Processes and Recipes for Enhanced, in situ CO2 Capture and Storage. Annu. Rev. Earth Planet. Sci. 39, 545–576. https://doi.org/10.1146/annurev-earth-092010-152509

Kelemen, P.B., McQueen, N., Wilcox, J., Renforth, P., Dipple, G., Vankeuren, A.P., 2020. Engineered carbon mineralization in ultramafic rocks for CO_2 removal from air: Review and new insights. Chem. Geol. 550, 119628. https://doi.org/10.1016/j.chemgeo.2020.119628

Köhler, P., Hartmann, J., Wolf-Gladrow, D.A., 2010. Geoengineering potential of artificially enhanced silicate weathering of olivine. Proc. Natl. Acad. Sci. U. S. A. 107, 20228–20233. https://doi.org/10.1073/pnas.1000545107

Kumar, A., Shrivastava, J.P., Pathak, V., 2017. Mineral carbonation reactions under water-saturated, hydrothermal-like conditions and numerical simulations of CO_2 sequestration in tholeiitic basalt of the Eastern Deccan Volcanic Province, India. Appl. Geochemistry 84, 87–104. https://doi.org/10.1016/j.apgeochem.2017.05.021

Lacinska, A.M., Styles, M.T., Bateman, K., Hall, M., Brown, P.D., 2017. An experimental study of the carbonation of serpentinite and partially serpentinised peridotites. Front. Earth Sci. 5. https://doi.org/10.3389/feart.2017.00037

Liu, D., Agarwal, R., Li, Y., Yang, S., 2019. Reactive transport modeling of mineral carbonation in unaltered and altered basalts during CO_2 sequestration. Int. J. Greenh. Gas Control 85, 109–120. https://doi.org/10.1016/j.ijggc.2019.04.006

Liu, D., Agarwal, R., Liu, F., Yang, S., Li, Y., 2022. Modeling and assessment of CO_2 geological storage in the Eastern Deccan Basalt of India. Environ. Sci. Pollut. Res. https://doi.org/10.1007/s11356-

022-21757-y

Lowson, R.T., Comarmond, M.C.J., Rajaratnam, G., Brown, P.L., 2005. The kinetics of the dissolution of chlorite as a function of pH and at 25°C. Geochim. Cosmochim. Acta 69, 1687–1699. https://doi.org/10.1016/j.gca.2004.09.028

Lu, X., Carroll, K.J., Turvey, C.C., Dipple, G.M., 2022. Rate and capacity of cation release from ultramafic mine tailings for carbon capture and storage. Appl. Geochemistry 140, 105285. https://doi.org/10.1016/j.apgeochem.2022.105285

Malmström, M., Banwart, S., Lewenhagen, J., Duro, L., Bruno, J., 1996. The dissolution of biotite and chlorite at 25°C in the near-neutral pH region. J. Contam. Hydrol. 21, 201–213. https://doi.org/10.1016/0169-7722(95)00047-X

Marieni, C., Matter, J.M., Teagle, D.A.H., 2020. Experimental study on mafic rock dissolution rates within CO_2-seawater-rock systems. Geochim. Cosmochim. Acta 272, 259–275. https://doi.org/10.1016/j.gca.2020.01.004

Marieni, C., Oelkers, E., 2018. Carbon sequestration potential of altered mafic reservoirs. Energy Procedia 146, 68–73. https://doi.org/https://doi.org/10.1016/j.egypro.2018.07.010

Marieni, C., Voigt, M.J., Oelkers, E.H., 2021. Experimental study of epidote dissolution rates from pH 2 to 11 and temperatures from 25 to 200 °C. Geochim. Cosmochim. Acta 294, 70–88. https://doi.org/10.1016/j.gca.2020.11.015

Marini, L., 2007. Chapter 6: The kinetics of mineral carbonation, in: Geological Sequestration of Carbon Dioxide. p. 470. https://doi.org/10.1016/S0921-3198(06)80026-8

Marty, N.C.M., Cama, J., Sato, T., Chino, D., Villiéras, F., Razafitianamaharavo, A., Brendlé, J., Giffaut, E., Soler, J.M., Gaucher, E.C., Tournassat, C., 2011. Dissolution kinetics of synthetic Na-smectite. An integrated experimental approach. Geochim. Cosmochim. Acta 75, 5849–5864. https://doi.org/10.1016/j.gca.2011.06.037

Matter, J.M., Stute, M., Snæbjörnsdóttir, S.Ó., Oelkers, E.H., Gislason, S.R., Aradottir, E., Sigfusson, B., Gunnarsson, I., Sigurdardottir, H., Gunnlaugsson, E., Axelsson, G., Alfredsson, H.A., Wolff-Boenisch, D., Mesfin, K., Taya, D.F. de la R., Hall, J., Dideriksen, K., Broecker, W.S., 2016. Rapid carbon mineralization for permanent disposal of anthropogenic carbon dioxide emissions. Science 352, 1312 LP – 1314. https://doi.org/10.1126/science.aad8132

Mayes, W.M., Riley, A.L., Gomes, H.I., Brabham, P., Hamlyn, J., Pullin, H., Renforth, P., 2018. Atmospheric CO2 Sequestration in Iron and Steel Slag: Consett, County Durham, United Kingdom. Environ. Sci. Technol. 52, 7892–7900. https://doi.org/10.1021/acs.est.8b01883

McGrail, B.P., Schaef, H.T., Ho, A.M., Chien, Y.J., Dooley, J.J., Davidson, C.L., 2006. Potential for carbon dioxide sequestration in flood basalts. J. Geophys. Res. Solid Earth 111, 1–13. https://doi.org/10.1029/2005JB004169

McGrail, B.P., Schaef, H.T., Spane, F.A., Horner, J.A., Owen, A.T., Cliff, J.B., Qafoku, O., Thompson, C.J., Sullivan, E.C., 2017. Wallula Basalt Pilot Demonstration Project: Post-injection Results and Conclusions. Energy Procedia 114, 5783–5790. https://doi.org/10.1016/j.egypro.2017.03.1716

Mehegan, J.M., Robinson, P.T., Delaney, J.R., 1982. Secondary mineralization and hydrothermal alteration in the Reydarfjordur drill core, eastern Iceland. J. Geophys. Res. 87, 6511–6524. https://doi.org/10.1029/JB087iB08p06511

Menefee, A.H., Giammar, D.E., Ellis, B.R., 2018. Permanent CO_2 Trapping through Localized and Chemical Gradient-Driven Basalt Carbonation. Environ. Sci. Technol. 52, 8954–8964.

https://doi.org/10.1021/acs.est.8b01814

Meysman, F.J.R., Montserrat, F., 2017. Negative CO_2 emissions via enhanced silicate weathering in coastal environments. Biol. Lett. 13. https://doi.org/10.1098/rsbl.2016.0905

Murray, R.S., Quirk, J.P., 1990. Surface Area of Clays. Langmuir 6, 122–124. https://doi.org/10.1021/la00091a018

National Academies of Sciences Engineering and Medicine, 2019. Negative Emissions Technologies and Reliable Sequestration. National Academies Press, Washington, D.C. https://doi.org/10.17226/25259

Nesbitt, H.W., Wilson, R.E., 1992. Recent chemical weathering of basalts. Am. J. Sci. 292, 740–777. https://doi.org/10.2475/ajs.292.10.740

Oelkers, E.H., 2001. An experimental study of forsterite dissolution rates as a function of temperature and aqueous Mg and Si concentrations. Chem. Geol. 175, 485–494. https://doi.org/10.1016/S0009-2541(00)00352-1

Oelkers, E.H., Gislason, S.R., 2001. The mechanism, rates and consequences of basaltic glass dissolution: I. An experimental study of the dissolution rates of basaltic glass as a function of aqueous Al, Si and oxalic acid concentration at 25°C and pH = 3 and 11. Geochim. Cosmochim. Acta 65, 3671–3681. https://doi.org/10.1016/S0016-7037(01)00664-0

Oelkers, E.H., Gislason, S.R., Matter, J., 2008. Mineral carbonation of CO_2. Elements 4, 333–337. https://doi.org/10.2113/gselements.4.5.333

Oelkers, E.H., Golubev, S. V., Chairat, C., Pokrovsky, O.S., Schott, J., 2009. The surface chemistry of multi-oxide silicates. Geochim. Cosmochim. Acta 73, 4617–4634. https://doi.org/10.1016/j.gca.2009.05.028

Oelkers, E.H., Schott, J., 2005. Geochemical aspects of CO_2 sequestration. Chem. Geol. 217, 183–186. https://doi.org/10.1016/j.chemgeo.2004.12.006

Oelkers, E.H., Schott, J., 2001. An experimental study of enstatite dissolution rates as funcion of pH, temperature, and aqueous Mg and Si concentration, and the mechanism of pyroxene/pyroxenoid dissolution. Geochim. Cosmochim. Acta 65, 1219–1231. https://doi.org/10.1016/S0016-7037(00)00564-0

Oelkers, E.H., Schott, J., Devidal, J.L., 1994. The effect of aluminum, pH, and chemical affinity on the rates of aluminosilicate dissolution reactions. Geochim. Cosmochim. Acta 58, 2011–2024. https://doi.org/10.1016/0016-7037(94)90281-X

Okoko, G.O., Olaka, L.A., 2021. Can East African rift basalts sequester CO2? Case study of the Kenya rift. Sci. African 13, e00924. https://doi.org/10.1016/j.sciaf.2021.e00924

Óskarsson, B. V., Riishuus, M.S., 2013. The mode of emplacement of Neogene flood basalts in Eastern Iceland: Facies architecture and structure of the Hólmar and Grjótá olivine basalt groups. J. Volcanol. Geotherm. Res. 267, 92–118. https://doi.org/10.1016/j.jvolgeores.2013.09.010

Oskierski, H.C., Dlugogorski, B.Z., Jacobsen, G., 2013. Sequestration of atmospheric CO_2 in chrysotile mine tailings of the Woodsreef Asbestos Mine, Australia: Quantitative mineralogy, isotopic fingerprinting and carbonation rates. Chem. Geol. 358, 156–169. https://doi.org/10.1016/j.chemgeo.2013.09.001

Palandri, J.L., Kharaka, Y.K., 2004. A compilation of rate parameters of water-mineral interaction kinetics for application to geochemical modeling. USGS Open File Rep. 2004–1068, 71.

Pan, S.Y., Chung, T.C., Ho, C.C., Hou, C.J., Chen, Y.H., Chiang, P.C., 2017. CO_2 Mineralization and Utilization using Steel Slag for Establishing a Waste-to-Resource Supply Chain. Sci. Rep. 7, 1–11. https://doi.org/10.1038/s41598-017-17648-9

Parkhurst, D.L., Appelo, C. a. J., 2013. Description of Input and Examples for PHREEQC Version 3 — A Computer Program for Speciation , Batch-Reaction , One-Dimensional Transport , and Inverse Geochemical Calculations, in: U.S. Geological Survey Techniques and Methods, Book 6, Chapter A43. pp. 6-43A.

Power, I.M., Dipple, G.M., Bradshaw, P.M.D., Harrison, A.L., 2020. Prospects for CO2 mineralization and enhanced weathering of ultramafic mine tailings from the Baptiste nickel deposit in British Columbia, Canada. Int. J. Greenh. Gas Control 94, 102895. https://doi.org/10.1016/j.ijggc.2019.102895

Ragnarsdóttir, K.V., 1993. Dissolution kinetics of heulandite at pH 2-12 and 25°C. Geochim. Cosmochim. Acta 57, 2439–2449. https://doi.org/10.1016/0016-7037(93)90408-O

Rigopoulos, I., Harrison, A.L., Delimitis, A., Ioannou, I., Efstathiou, A.M., Kyratsi, T., Oelkers, E.H., 2018. Carbon sequestration via enhanced weathering of peridotites and basalts in seawater. Appl. Geochemistry 91, 197–207. https://doi.org/10.1016/j.apgeochem.2017.11.001

Robinson, P.T., Hall, M., Christensen, N.I., Gibson, I.A.N.L., Schmincke, H., 1982a. The Iceland Research Drilling Project: Synthesis of results and implications for the nature of Icelandic and oceanic crust 87, 6657–6667.

Robinson, P.T., Mehegan, J., Gibson, I.L., Schmincke, H.U., 1982b. Lithology and structure of the volcanic sequence in eastern Iceland. J. Geophys. Res. 87, 6429–6436. https://doi.org/10.1029/JB087iB08p06429

Ross, G.J., 1967. Kinetics of acid dissolution of an orthochlorite mineral. Can. J. Chem. 45, 3031–3034. https://doi.org/10.1139/v67-491

Rozalén, M.L., Huertas, F.J., Brady, P. V., Cama, J., García-Palma, S., Linares, J., 2008. Experimental study of the effect of pH on the kinetics of montmorillonite dissolution at 25 °C. Geochim. Cosmochim. Acta 72, 4224–4253. https://doi.org/10.1016/j.gca.2008.05.065

Sanders, R.L., Washton, N.M., Mueller, K.T., 2010. Measurement of the reactive surface area of clay minerals using solid-state NMR studies of a probe molecule. J. Phys. Chem. C 114, 5491–5498. https://doi.org/10.1021/jp906132k

Savage, D., Cave, M.R., Haigh, D., Milodowski, A.E., Young, M.E., 1993. The reaction kinetics of laumontite under hydrothermal conditions. Eur. J. Mineral. 5, 523–536. https://doi.org/10.1127/ejm/5/3/0523

Schaef, H.T., McGrail, B.P., 2009. Dissolution of Columbia River Basalt under mildly acidic conditions as a function of temperature: Experimental results relevant to the geological sequestration of carbon dioxide. Appl. Geochemistry 24, 980–987. https://doi.org/10.1016/j.apgeochem.2009.02.025

Schaef, H.T., McGrail, B.P., Owen, A.T., 2010. Carbonate mineralization of volcanic province basalts. Int. J. Greenh. Gas Control 4, 249–261. https://doi.org/10.1016/j.ijggc.2009.10.009

Schott, J., Pokrovsky, O.S., Oelkers, E.H., 2009. The link between mineral dissolution/precipitation kinetics and solution chemistry. Rev. Mineral. Geochemistry 70, 207–258. https://doi.org/10.2138/rmg.2009.70.6

Shrivastava, J.P., Rani, N., Pathak, V., 2016. Geochemical modeling and experimental studies on

mineral carbonation of primary silicates for long-term immobilization of CO_2 in basalt from the eastern Deccan volcanic province. Jour. Indian Geophys. Union, Sp 1, 42–58.

Snæbjörnsdóttir, S.Ó., Oelkers, E.H., Mesfin, K., Aradóttir, E.S., Dideriksen, K., Gunnarsson, I., Gunnlaugsson, E., Matter, J.M., Stute, M., Gislason, S.R., 2017. The chemistry and saturation states of subsurface fluids during the in situ mineralisation of CO_2 and H_2S at the CarbFix site in SW-Iceland. Int. J. Greenh. Gas Control 58, 87–102. https://doi.org/10.1016/j.ijggc.2017.01.007

Snæbjörnsdóttir, S.Ó., Sigfússon, B., Marieni, C., Goldberg, D., Gislason, S.R., Oelkers, E.H., 2020. Carbon dioxide storage through mineral carbonation. Nat. Rev. Earth Environ. https://doi.org/10.1038/s43017-019-0011-8

Stubbs, A.R., Paulo, C., Power, I.M., Wang, B., Zeyen, N., Wilson, S.A., 2022. Direct measurement of CO_2 drawdown in mine wastes and rock powders: Implications for enhanced rock weathering. Int. J. Greenh. Gas Control 113, 103554. https://doi.org/10.1016/j.ijggc.2021.103554

Tester, J.W., Worley, W.G., Robinson, B.A., Grigsby, C.O., Feerer, J.L., 1994. Correlating quartz dissolution kinetics in pure water from 25 to 625°C. Geochim. Cosmochim. Acta 58, 2407–2420. https://doi.org/10.1016/0016-7037(94)90020-5

Turvey, C.C., Wilson, S.A., Hamilton, J.L., Tait, A.W., McCutcheon, J., Beinlich, A., Fallon, S.J., Dipple, G.M., Southam, G., 2018. Hydrotalcites and hydrated Mg-carbonates as carbon sinks in serpentinite mineral wastes from the Woodsreef chrysotile mine, New South Wales, Australia: Controls on carbonate mineralogy and efficiency of CO_2 air capture in mine tailings. Int. J. Greenh. Gas Control 79, 38–60. https://doi.org/10.1016/j.ijggc.2018.09.015

Valdés, M.G., Pérez-Cordoves, A.I., Díaz-García, M.E., 2006. Zeolites and zeolite-based materials in analytical chemistry. TrAC - Trends Anal. Chem. 25, 24–30. https://doi.org/10.1016/j.trac.2005.04.016

Voigt, M., Marieni, C., Clark, D.E., Gíslason, S.R., Oelkers, E.H., 2018. Evaluation and refinement of thermodynamic databases for mineral carbonation. Energy Procedia 146, 81–91. https://doi.org/10.1016/j.egypro.2018.07.012

Walker, G.P.L., 1958. Geology of the reydarfjördur area, Eastern Iceland. Q. J. Geol. Soc. London 114, 367–391. https://doi.org/10.1144/gsjgs.114.1.0367

Walker, J.C.G., Hays, P.B., Kasting, J.F., 1981. A negative feedback mechanismfor the long-term stabilization of earth's surface temperature. J. Geophys. Res. 86, 9776–9782.

Wilson, S.A., Harrison, A.L., Dipple, G.M., Power, I.M., Barker, S.L.L., Ulrich Mayer, K., Fallon, S.J., Raudsepp, M., Southam, G., 2014. Offsetting of CO_2 emissions by air capture in mine tailings at the Mount Keith Nickel Mine, Western Australia: Rates, controls and prospects for carbon neutral mining. Int. J. Greenh. Gas Control 25, 121–140. https://doi.org/10.1016/j.ijggc.2014.04.002

Wolff-Boenisch, D., Gislason, S.R., Oelkers, E.H., 2006. The effect of crystallinity on dissolution rates and CO2 consumption capacity of silicates. Geochim. Cosmochim. Acta 70, 858–870. https://doi.org/10.1016/j.gca.2005.10.016

Wu, Y., Li, P., 2020. The potential of coupled carbon storage and geothermal extraction in a CO_2-enhanced geothermal system: a review. Geotherm. Energy 8. https://doi.org/10.1186/s40517-020-00173-w

Yates, D.J.C., 1968. Studies on the surface area of zeolites, as determined by physical adsorption and X-ray crystallography. Can. J. Chem. 46, 1695–1701. https://doi.org/10.1139/v68-282